



Improvements to the representation of BVOC chemistry-climate interactions in UKCA (vn11.5) with the CRI-Strat 2 mechanism: Incorporation and Evaluation

James Weber¹, Scott Archer-Nicholls¹, Nathan Luke Abraham^{1,2}, Youngsub M. Shin¹, Thomas J. Bannan³, Carl J. Percival⁴, Asan Bacak⁵, Paulo Artaxo⁶, Michael Jenkin⁷, M. Anwar H. Khan⁸, Dudley E. Shallcross⁸, Rebecca H. Schwantes^{9,10}, Jonathan Williams^{11,12}, Alex T. Archibald^{1,2}

Correspondence to: James Weber (jmw240@cam.ac.uk)

¹Centre for Atmospheric Science, Department of Chemistry, University of Cambridge, Cambridge, CB2 1EW, UK

²National Centre for Atmospheric Science, Department of Chemistry, University of Cambridge, CB2 1EW, UK

³School of Earth and Environmental Sciences, University of Manchester, Manchester, M13 9PL, UK

⁴NASA Jet Propulsion Laboratory, California Institute of Technology, 4800 Oak Grove Drive, Pasadena, CA 91109, USA.

⁵Turkish Accelerator & Radiation Laboratory, Ankara University Institute of Accelerator Technologies, Gölbaşı Campus, 06830 Gölbaşı, Ankara, Turkey.

⁶Physics Institute, University of São Paulo, Rua do Matão 1371, CEP 05351-015, São Paulo, Brazil

⁷Atmospheric Chemistry Services, Okehampton, Devon, EX20 4BQ, UK

⁸Biogeochemistry Research Centre, School of Chemistry, University of Bristol, Cantock's Close, Bristol, BS8 1TS, UK

⁹Chemical Sciences Laboratory, National Oceanic and Atmospheric Administration, Boulder, CO 80305, USA

¹⁰Cooperative Institute for Research in Environmental Sciences, University of Colorado, Boulder, CO, 80309, USA

¹¹Department of Atmospheric Chemistry, Max Planck Institute for Chemistry, Mainz, 55128, Germany.

¹²Energy, Environment and Water Research Center, The Cyprus Institute, Nicosia, Cyprus

Abstract We present the first incorporation of the Common Representative Intermediates version 2.2 tropospheric chemistry mechanism, CRI v2.2, combined with stratospheric chemistry, into the global chemistry-climate United Kingdom Chemistry and Aerosols (UKCA) model to give the CRI-Strat 2 mechanism. A rigorous comparison of CRI-Strat 2 with the earlier version, CRI-Strat, is performed in UKCA in addition to an evaluation of three mechanisms, CRI-Strat 2, CRI-Strat and the standard UKCA chemical mechanism, StratTrop vn1.0, against a wide array of surface and airborne chemical data.

CRI-Strat 2 comprises a state-of-the-art isoprene scheme, optimised against the MCM v3.3.1, which includes isoprene peroxy radical isomerisation, HO_x-recycling through the addition of photolabile hydroperoxy aldehydes (HPALDs) and IEPOX formation. CRI-Strat 2 also features updates to several rate constants for the inorganic chemistry including the reactions of inorganic nitrogen and O(¹D).



The update to the isoprene chemistry in CRI-Strat 2 increases OH over the lowest 500m in tropical forested regions by 30-50%, relative to CRI-Strat, leading to an improvement in model-observation comparisons for surface OH and isoprene relative to CRI-Strat and StratTrop. Enhanced oxidants also cause a 25% reduction in isoprene burden and an increase in oxidation fluxes of isoprene and other biogenic volatile organic compounds (BVOCs) at low altitudes with likely impacts on subsequent atmospheric lifetime, aerosol formation and climate.

By contrast, updates to the rate constants of $O(^1D)$ with its main reactants relative to CRI-Strat reduces OH in much of the free troposphere, producing a 2% increase in the methane lifetime, and increases the tropospheric ozone burden by 8%, primarily from reduced loss via $O(^1D) + H_2O$. The changes to inorganic nitrogen reaction rate constants increase the NO_x burden by 4% and shift the distribution of nitrated species closer to that simulated by StratTrop.

CRI-Strat 2 is suitable for multi-decadal model integrations and the improved representation of isoprene chemistry provides an opportunity to explore the consequences of HO_x -recycling in the United Kingdom Earth System Model (UKESM1). This new mechanism will enable a re-evaluation of the impact of BVOCs on the chemical composition of the atmosphere and probe further the feedback between the biosphere and the climate.

1. Introduction

Isoprene (2-methyl-1,3-butadiene) makes up 70 % of all non-methane BVOC emissions with annual average emissions of 594 ± 34 Tg/year over the period 1980-2010 (Sindelarova et al., 2014). Isoprene's rapid chemical oxidation in the atmosphere by OH, O_3 and NO_3 directly affects the tropospheric oxidising capacity, ozone burden and the processing of other trace gases like methane (e.g. Archibald et al., 2011) while also serving as an important source of secondary organic aerosol (SOA) (e.g., Kelly et al., 2018). Thus, isoprene has substantial effects on the radiative balance of the atmosphere, both directly via production of SOA and ozone, and indirectly via its changes to the oxidising capacity of the atmosphere influencing methane lifetime and production of other aerosol species such as from oxidation of monoterpenes and SO_2 . An accurate representation of isoprene's chemical behaviour in climate models is essential to understanding the feedbacks between the biosphere and the rest of the Earth system and thus capturing isoprene's climatic impact.

However, the treatment of isoprene in the chemistry schemes of many climate models is outdated or oversimplified (e.g. Squire et al., 2015). The last decade has seen significant advances in our understanding of the isoprene oxidation pathway, principally the concept of rapid, intramolecular hydrogen shifts (H-shifts), also termed isomerisation reactions, in the isoprene hydroxy peroxy radicals (frequently termed ISOPOO). Predictions from theoretical work (Peeters et al., 2009, Peeters et al., 2014) and observations (Crounse et al., 2011; Teng et al., 2017; Wennberg et al., 2018) have established this pathway to be competitive with the traditional bimolecular reactions of the peroxy radical with NO , NO_3 , HO_2 and RO_2 in certain conditions such as low $NO_x (=NO + NO_2)$ environments. These H-shifts reactions lead to the production of $HO_x (=OH + HO_2)$ either directly or indirectly following the degradation of the isomerisation products (e.g., Archibald et al., 2010, Jenkin et al., 2015, Wennberg et al., 2018).



This process, termed HO_x-recycling, has been shown to be important for low-NO_x, high-isoprene regions of the atmosphere (Butler et al., 2008, Lelieveld et al., 2008). By adding a simple, fixed yield OH production pathway from ISOPOO to represent OH production from hydroperoxy aldehydes (HPALDs), Archibald et al (2011) simulated an 18% increase in tropospheric O₃ burden while the tropospheric OH burden increased by 17% in the present day (PD) and by 50% in a pre-industrial (PI) atmosphere featuring 1860 emissions of key chemical species such as NO_x, CO and isoprene. Consequently, the lifetime of methane was predicted to decrease between 11% (in a future climate scenario) and 35% (in the PI). This illustrated the significant impact that such a process could have on our understanding of the PI atmosphere (and the radiatively active components therein), and thus the PD-PI change and climate sensitivity. While the greatest change to the chemistry was simulated in the boundary layer (BL), convection of isoprene and its oxidation products into the free troposphere resulted in this added chemistry having global impacts. The effect on oxidants from HO_x-recycling influences the lifetimes of isoprene and other BVOCs such as monoterpenes and thus the extent of their dispersion and the location of the subsequent SOA formation. Karset et al. (2018) found that when lower oxidant fields were applied to the PI atmosphere isoprene, monoterpenes, SO₂ and other key aerosol precursors were more dispersed from their sources, reaching higher altitudes and enhancing particle number concentration in the remote free troposphere. The radiative impact of the resulting aerosols was greater due to their enhanced lifetime (from slower deposition) and the highly non-linear relationship between aerosol number and cloud forcing where the addition of a given concentration of aerosol has a much greater impact in remote regions where the background concentration of aerosol is smaller (Chen et al., 2016). The importance of oxidants to BVOCs and aerosol was also shown in Sporre et al (2020) where models with an interactive oxidant scheme simulated a BVOC-driven depletion of oxidants and attendant greater dispersion of BVOCs and their oxidation products (including SOA precursors). In contrast, a prescribed oxidant approach saw BVOC oxidation confined far more to source regions, reducing dispersion.

Change to oxidant fields also perturb the oxidation pathways of SO₂. In the United Kingdom Chemistry and Aerosols (UKCA) model, SO₂ can be oxidised in the gas phase by OH to yield H₂SO₄ or in the aqueous phase by O₃ or H₂O₂ (Mulcahy et al., 2020). This has consequences for the aerosol mass and number distributions because only H₂SO₄ can nucleate new particles in UKCA, therefore amplifying the gas phase pathway over the aqueous pathways leads to a greater number of smaller aerosols. Thus, uneven changes to these pathways can alter the size and number distribution of the aerosol population, affecting the radiative properties of aerosols and clouds. Decreases in OH in other UKCA studies (Weber et al., 2020a, O'Connor et al., 2020) have resulted in simulated reductions in particle number concentration and cloud droplet number concentration. The resulting negative cloud radiative forcing is smaller in magnitude as the lower cloud droplet number concentration (CDNC) makes the clouds less “bright” (Twomey et al., 1974). The impact of different oxidant schemes on the burden and lifetime of DMS, an important SO₂ precursor, and the impact to sulphate aerosol transport is highlighted by Mulcahy et al. (2020).

While Archibald et al (2011) used a relatively simple approach to simulate HO_x-recycling, further advances in the chemical understanding have led to a near explicit representation of HO_x-recycling being incorporated into comprehensive mechanisms including the Master Chemical Mechanism (MCM v3.3.1) (Jenkin et al., 2015) and the



111 CalTech isoprene scheme (Wennberg et al., 2018). However, such mechanisms are far too large for use in global
 112 chemistry-climate models.

113

114 There exist a few reduced mechanisms featuring this state-of-the-art isoprene chemistry suitable for use in chemistry-
 115 climate models including the CalTech reduced isoprene scheme (Bates et al., 2019) and the Common Representative
 116 Intermediates mechanism v2.2 (CRI v2.2) (Jenkin et al., 2019), the focus of this work. The CRI v2.2 is an update to
 117 the Common Representative Intermediate v2.1 mechanism (Jenkin et al., 2008, Utembe et al., 2009, Watson et al.,
 118 2008) and was developed from the fully explicit Master Chemical Mechanism (MCM) version 3.3.1 (Jenkin et al.,
 119 2015) which describes the degradation of organic compounds in the troposphere. In the CRI framework, species are
 120 lumped together into surrogate molecules whose behaviour is optimised against the fully explicit MCM. A description
 121 of CRI v2.2 is given in Jenkin et al. (2019). The CRI v2.1, along with the corresponding stratospheric chemistry, has
 122 already been incorporated into UKCA as CRI-Start (CS) (Archer-Nicholls et al., 2020) as an alternative to the simpler
 123 but more widely used STRAT-TROP (ST) chemistry scheme (Archibald et al., 2020a), the scheme used for UKESM's
 124 contributions to CMIP6 (e.g. Sellar et al., 2020, Thornhill et al., 2020).

125

126 Using the reduced Caltech Isoprene Mechanism, which includes H-shifts of ISOPOO in GEOS-CHEM, Bates et al
 127 (2019) simulated significant increases in OH (>100%) and HO₂ (up to 50%) over the Amazon and other forested
 128 tropical regions as a result of the HO_x-recycling. After implementing updated rate constants for isoprene H-shifts in
 129 GEOS-CHEM Möller et al. (2019) also found that globally around 30% of all isoprene peroxy radicals undergo at
 130 least one H-shift reaction resulting in an OH yield of 47% per isoprene molecule and that adding all isoprene H-shift
 131 reactions increased boundary layer OH by up to a factor of three in the Amazon. Using CESM/CAM-CHEM and the
 132 MOZART-TS2 mechanism, Schwantes et al (2020) showed reasonable agreement for some isoprene oxidation
 133 products over the Southeast USA.

134

135 Jenkin et al. (2019), using CRI v2.2 in the STOCHEM Lagrangian chemistry-transport model, showed the significant
 136 influence of HO_x recycling in CRI v2.2 simulating a 6.4% increase in the tropospheric OH burden relative to the CRI
 137 v2.1 and increases of surface OH of 20-50% over much of the forested tropical regions. Khan et al. (2021), using the
 138 same setup, also simulated enhanced surface OH and attendant decreases in methane lifetime (0.5 years) and isoprene
 139 burden (17%).

140

141 However, while the reduced mechanisms featuring HO_x-recycling chemistry have been tested in chemistry-climate
 142 models, less work has been done in terms of multi-species comparison to observations and detailed analysis of the
 143 effect to global atmospheric composition. This study introduces the CS2, based on CRIv2.2 and expanded with
 144 stratospheric chemistry, as a mechanism in UKCA, evaluates its performance against observational data, and
 145 compares its output and key processes to the related CS mechanism and well-established ST mechanism. By
 146 providing a wide-ranging comparison to observations and a detailed description of the changes CS2 causes to global
 147 and regional atmospheric chemistry, this current work builds on the existing literature to develop further our
 148 understanding of the consequences of HO_x-recycling.



149 2. Development of CS2 - incorporation of CRI v2.2 into UKCA

150

151 It is important to note that the CRI v2.2 mechanism, like the CRI v2.1 mechanism, is strictly a tropospheric chemistry
 152 scheme. In developing the whole atmosphere mechanism CS, Archer-Nicholls et al (2020) merged the CRI v2.1
 153 mechanism with the Stratospheric chemistry scheme (Morgenstern et al., 2009) in UKCA (Table 1) to allow this
 154 scheme to be used within UKESM1 (Sellar et al., 2019). The same approach was taken in this work with the
 155 Stratospheric scheme unchanged and tropospheric scheme switched from CRI v2.1 to CRI v2.2. Therefore, to
 156 differentiate the “CRI v2.2” mechanism used in UKCA in this work from the solely tropospheric CRI v2.2 mechanism
 157 described on the CRI v2.2 website (<http://cri.york.ac.uk/>), the UKCA mechanism will henceforth be referred to as
 158 CRI-Strat 2 (CS2) (Table 1). A full description of the changes made to CS to update it to CS2 is given in the supplement
 159 Section 1.1 while a summary of the changes is now discussed.

160

161 CS2 features a significant update to isoprene oxidation chemistry relative to CS with the incorporation of 1,6 and 1,4
 162 H-shift reactions of isoprene peroxy radicals as well as an update to the organonitrate scheme (as detailed in Jenkin
 163 et al., 2019). CS2 also features updates to multiple reaction rate constants (which were out of date in CS (Archer-Nicholls
 164 et al., 2020)) to the best of our understanding as documented in the IUPAC Task Group on Atmospheric Chemical
 165 Kinetic Data Evaluation (<http://iupac.pole-ether.fr/>). Changes to the rate constants of the reactions of O(¹D) with H₂O,
 166 O₂ and N₂; rate constants of multiple inorganic nitrogen reactions such as those forming PAN-type species, HONO₂
 167 and the HO₂+NO reaction and the rate constants of organic peroxy radicals (RO₂) with NO and NO₃. These updates
 168 ensure consistency between the CS2 mechanism incorporated in UKCA and that described on the CRI v2.2 website
 169 (<http://cri.york.ac.uk/>). The photolysis of glyoxal, formaldehyde and propionaldehyde was also updated (see SI
 170 Section S6).

171

172 CS2 has 9 more species than CS (Tables 1, 2) as well as 46 additional bimolecular reactions, 12 additional photolysis
 173 reactions and 8 additional uni/termolecular reactions (Table 1). This leads to a modest increase in runtime (6%)
 174 compared with CS whose runtime was already ~75% greater than ST. Incorporation of CS2 into UKCA involved
 175 extensive use of the UM-UKCA virtual machine environment (Abraham et al., 2018).

176

177 The main update to the isoprene chemistry is the inclusion of 1,6 and 1,4 H-shift reactions of the isoprene peroxy
 178 radical (termed RU14O2 in CRI nomenclature). The 1,6 H-shift process is well studied (Peeters et al., 2009, Crounse
 179 et al., 2011, Teng et al., 2017, Wennberg et al., 2018) and follows the $k_{bulk1,6H}$ rate coefficient described in Jenkin et
 180 al. (2019), capturing the dependence of isomerisation on both temperature and the rates of reaction of RU14O2 with
 181 the standard bimolecular partners (NO, NO₃, HO₂ and RO₂). This pathway yields hydroperoxy aldehydes (HPALDs,
 182 termed HPUCARB12 in CS2) and dihydroperoxy carbonyls peroxy radicals (DHPR12O2). The photolysis of the
 183 highly photolabile HPALD (HPUCARB12), and its product HUCARB9 (unsaturated hydroxy carbonyl), are key
 184 routes for HO_x regeneration.

185



186 The production of the isoprene epoxy diol (IEPOX) from the isoprene hydroperoxide (RU14OOH) and the
 187 hydroxymethyl-methyl- α -lactone (HMML) also represent important updates (Jenkin et al., 2019). IEPOX and HMML
 188 are known SOA precursors (Nguyen et al., 2014; Nguyen et al 2015; Allan et al., 2014) and so their addition may
 189 enable a more explicit representation of SOA formation within the CRI framework, as opposed to the current
 190 framework whereby SOA formation is represented by the condensation on existing aerosol of a single inert tracer,
 191 Sec_Org, which is made from monoterpene oxidation (Mann et al., 2010; Mulcahy et al., 2020). This is beyond the
 192 scope of this paper but will be a focus of future work.

193

194 The introduction of HPUCARB12 and HUCARB9 necessitates a careful update to the FASTJX photolysis scheme
 195 used by UKCA (Telford et al., 2013). The cross-sectional dependence of wavelength for HPALDs is assumed to be
 196 the same as methacrolein (Peeters et al., 2009, Wennberg et al., 2018, Schwantes et al., 2020) but with a significantly
 197 larger quantum yield (QY). Prather et al (2013) recommends a QY of 0.003 for methacrolein and Liu et al (2017) a
 198 QY of 0.55 for HPALDs (both used by Wennberg et al., 2018). To implement the photolysis of these new species, the
 199 photolysis frequencies of HPUCARB12 was taken to be the photolysis frequency for methacrolein scaled by the ratio
 200 of the QY of HPALDs to the QY of methacrolein, the same approach used by Schwantes et al (2020) for δ -HPALDs.
 201 A scaling of 0.5 was applied to the photolysis frequency of HUCARB9 in agreement with the MCM v3.3.1.

202

203 In addition to the updates to isoprene chemistry, CRIV2.2 has had the rate coefficients for many organic and inorganic
 204 reactions updated to bring the mechanism into agreement with the MCM v3.3.1 and IUPAC. These affect the overall
 205 chemistry in three major ways. The first involves the major reactions of the excited oxygen radical, O(¹D). The rate
 206 constants of O(¹D) with H₂O, O₂ and N₂ changed by -3%, -1% and +20% respectively to bring them into agreement
 207 with the current IUPAC values (<http://iupac.pole-ether.fr>). This also means the rate constant of O(¹D) with N₂ became
 208 much closer (within $\pm 1.5\%$) to that used in ST (Archibald et al., 2020a) and rate constants for the reactions with O₂
 209 and H₂O also move closer to those used by ST. The result of this is a reduction in the fraction of O(¹D) reacting with
 210 H₂O by 10-15%, thus lowering OH production while also reducing O_x loss via this pathway.

211

212 The second involves multiple inorganic reactions of nitrated species. The formation rate constants for PAN-type
 213 species (species with peroxyacyl nitrate functionality), HONO₂, HO₂NO₂ and N₂O₅ changed by around -45%, -15%,
 214 -45% and +50-75% in the troposphere respectively. The change for PAN brought its formation rate constant much
 215 closer to that used in ST (within $\pm 7\%$) and this was also the case for HONO₂ and HO₂NO₂ formation. The rate constant
 216 of HO₂ + NO, the single biggest production source of O_x, decreased by 4%.

217

218 Finally, the rate constants for most RO₂ + NO and RO₂ + NO₃ reactions have been changed by +12.5% and -8%,
 219 respectively while maintaining the same temperature dependence. This is likely to have a smaller impact than the other
 220 chemistry changes but, at the margins, will make reactions with NO more competitive with the isomerisation reactions
 221 of the ISOPOO.

222



The implementation of CRI v2.2 by Khan et al (2021) in STOCHEM model, while including the updates to isoprene chemistry and the $\text{RO}_2 + \text{NO}$ and $\text{RO}_2 + \text{NO}_3$ reactions, did not feature updates to the rate constants for $\text{O}(^1\text{D})$ with H_2O , O_2 and N_2 or the inorganic nitrogen reactions. Therefore, even in low altitude terrestrial conditions where isoprene HO_x -recycling tends to dominate the change in OH, comparison between Khan et al (2021) and the results of this work must be caveated with the changes to the inorganic chemistry.

In addition to the chemistry changes, updates are made to the photolysis of several species. Two additional photolysis reactions of glyoxal (CARB3 in the CRI mechanisms) were added as well as updates to the photolysis parameters for HCHO and EtCHO (propionaldehyde). The wavelength bins of the product of cross-section and quantum yield used by FAST-JX (Telford et al., 2013) used were updated to the v7.3 values from Prather et al (2015) for HCHO and $\text{C}_2\text{H}_5\text{CHO}$. The photolysis of CARB3, which had previously been estimated in CS by a scaling of HCHO photolysis (Archer-Nicholls et al., 2020), is replaced with the glyoxal photolysis for 999 hPa from v7.3 of Prather et al (2015). This reaction does exhibit a modest pressure dependence but one which has not been incorporated into FAST-JX at the current time.

In addition to the changes to the chemistry and photolysis, updates to the wet deposition scheme were implemented to both CS and CS2 schemes. The previous approach of applying parameters for standard surrogate for other species with the same functional groups (e.g. EtOOH was used for most hydroperoxides), as described in Archer-Nicholls et al (2020), was updated to use either data for the precise species (taken from Schwantes et al., 2020) or a more closely related-surrogate. The changes to the wet deposition parameters are detailed in Table S1 of the supplement and, as they were applied to both CS and CS2 mechanisms, they are unlikely to have a significant influence on the inter-mechanism difference. No changes were made to the dry deposition scheme in this work.

3. Model Runs

All model runs were performed using the United Kingdom Chemistry and Aerosols Model (UKCA) run at a horizontal resolution of $1.25^\circ \times 1.875^\circ$ with 85 vertical levels up to 85 km (Walters et al., 2019) and the GLOMAP-mode aerosol scheme which simulates sulfate, sea salt, BC, organic matter, and dust but not currently nitrate aerosol (Mulcahy et al., 2020). In this setup, the inert chemical tracer Sec_Org, which condenses irreversibly onto existing aerosol, was produced at a 26% yield solely from reactions of α -pinene and β -pinene with O_3 , OH and NO_3 with the enhanced yield applied to account for a lack of SOA formation from isoprene or anthropogenic species (Mulcahy et al., 2020).

The runs in this work fell into two distinct categories. Firstly, short runs (generally 1-2 months, Table 3) with higher frequency (hourly) output using the ST, CS and CS2 chemical mechanisms were performed to evaluate each mechanism's performance against the observational data. Secondly, longer runs (2-5 years, Table 4) with monthly output using the CS and CS2 chemical mechanisms (or variants of CS2 for sensitivity tests) were conducted to facilitate a rigorous comparison of the global chemical composition (Table 4).



Temperature and horizontal wind fields were nudged (Telford et al., 2008) in all model runs to atmospheric reanalyses from ECMWF (Dee et al., 2011) to constrain the simulations to consistent meteorology, thus preventing diverging meteorology adding to the differences resulting from the chemical mechanisms and replicating as closely as possible the atmospheric conditions experienced when the observations were recorded. Nudging only occurred above ~1200 m in altitude and thus the majority of the planetary boundary layer was not nudged. The model runs were atmosphere-only with prescribed sea surface temperatures (SSTs). CO₂ is not emitted but set to a constant field while methane, CFCs and N₂O are prescribed with constant lower boundary conditions, all at 2014 levels (Archibald et al., 2020a).

The emissions used in this study the same as those from Archer-Nicholls et al (2020) and are those developed for the Coupled-Model Intercomparison Project 6 (CMIP6) (Collins et al., 2017). Anthropogenic and biomass burning emissions data for CMIP6 are from the Community Emissions Data System (CEDS), as described by Hoesly et al. (2018). For the short runs, timeseries anthropogenic and biomass burning emissions were used for all ST runs and all CRI runs up to 2015. For the runs done for comparison to observational data recorded at the Z2F site new Manaus in 2016 (see Tables 3, 5), timeslice 2014 emissions were used due to a lack of post-2015 CRI emissions although the impact of the difference is expected to be minimal.

All longer runs used time slice 2014 emissions for anthropogenic and biomass burning emissions. Oceanic emissions were from the POET 1990 dataset (Olivier et al., 2003) and all biogenic emissions except isoprene and monoterpenes (see Section 3.3) were based on 2001-2010 climatologies from Model of Emissions of Gases and Aerosols from Nature under the Monitoring Atmospheric Composition and Climate project (MEGAN-MACC) (MEGAN) version 2.1 (Guenther et al., 2012) and are discussed further in Section 3.3. A full description of the emission sources for each emitted species is given in Table S2.

All mechanisms used the same raw emissions data. However, the additional emitted species required by CS and CS2 means the total mass of emitted organic compounds is greater in CS and CS2 and the lumping of species for emissions is also different. The approach and consequences are discussed in Archer-Nicholls et al (2020).

3.1 Short runs for model-observation comparisons

The runs performed for comparison to observations are detailed in Table 3 and correspond to an observational dataset described in Section 4 and Table 5. All runs were spun-up for a minimum of three months. For most of the runs, hourly model output was used so as to allow for detailed comparison with observations. The only exception were the runs performed for the comparison to the Isoprene Column data ("Isoprene Column" Table 3) where monthly means were used.

3.2 Longer runs for mechanistic intercomparison

The longer runs (Table 4) were designed with the primary aim of examining the consequences of the mechanism changes between CS and CS2 and followed an approach similar to that used by Archer-Nicholls et al (2020). These



runs also served a secondary purpose as they enabled longer term comparison to observations for several species. We ran two 5 years nudged runs (1 year spin up, 4 years analysis) with the CS and CS2 mechanisms. In addition, five 2-year sensitivity runs (1 year spin up, 1 year analysis) were performed to analyse the impact of the individual changes to the isoprene scheme, the O(¹D) reactions, inorganic nitrogen reactions, the RO₂+NO/NO₃ reactions and the photolysis reactions as discussed in Section 2. These sensitivity tests featured mechanisms based on the CS2 mechanism but each had a different feature which was reverted to that found in CS.

305

CS2_O1D used the old rate constants from CS for the reaction of O(¹D) with N₂, O₂ and H₂O. CS2_inorgN used the rate constants from CS for the formation of HONO₂, HO₂NO₂, PANs, HONO and N₂O₅ as well as for the reactions of HO₂ + NO, OH+MeONO₂, OH+ PAN and OH+MPAN.

309

CS2_isoprene followed as closely as possible the isoprene reactions from CS with the major change being the omission of the isomerisation reactions of RU14O2 and subsequent production of HPALDs and other species which are key for HO_x recycling.

313

In CS2_RO2_N, the rate constants for the RO₂ + NO and RO₂ + NO₃ reactions were reverted to those used in CS which led to a 12.5% decrease and 8% increase, respectively for the vast majority of these reactions. Where branching ratios changed between CS and CS2, the CS2 branching ratios were maintained and the rate constants scaled accordingly.

318

Finally, CS2_photo used the parameters and reactions from CS for the photolysis of CARB3 (glyoxal), HCHO and EtCHO and was performed to evaluate the impact of update to photolysis (see SI Section S6).

321

Each sensitivity test, when compared to the CS2 run, provides information as to the impact of the change of the respective section of the mechanism (when taken in isolation); for example, the impact of the changes to the rate coefficients of O(¹D)'s reactions is examined by comparing the CS2 and CS2_O1D runs.

325

A full description of the changes to reactions and rate constants for each sensitivity test is given in the supplement Section S2. The changes to the photolysis were found to have a minimal effect on atmospheric composition compared with the other sensitivity tests and is described entirely in the supplement. The analysis of the longer runs is discussed in Section 5.

330

331

3.3 Biogenic Emissions

This work used the interactive Biogenic Volatile Organic Compound (iBVOC) emissions system (Pacífico et al., 2012) for isoprene and monoterpenes, the standard approach for UKESM's contributions to CMIP6 (Sellar et al., 2019). Emissions of isoprene and monoterpenes are calculated interactively based on temperature, photosynthetically active radiation (PAR) and plant functional type for each grid cell. While a diel cycle for isoprene is standard in UKESM,



iBVOC has the advantage of also simulating a diel cycle of emissions for monoterpenes, leading to improved model performance relative to observation (see Section 4). The dependence on temperature and PAR means that emissions of BVOCs differ slightly between runs and thus between mechanisms. However, nudging inhibits considerably divergence of surface temperature between comparative runs and so the differences between emissions were <5% and typically 1-2%, significantly smaller than the differences caused by the mechanisms.

Monoterpenes emissions were speciated in a 2:1 α -pinene : β -pinene ratio as used in Archer-Nicholls et al (2020).

There are temporal and spatial disparities between using iBVOC emissions and offline emissions, such as the MEGAN-MACC dataset ((Sindelarova et al., (2014), as used by Archer-Nicholls et al., (2020)), which could affect conclusions about mechanism-observational biases. These differences are discussed in more detail in SI Section S. In short, for the ZF2 Brazil, ATTO and Borneo sites for the periods considered, the isoprene and MT emissions were higher when using the iBVOC approach than for MEGAN-MACC (Figs. S1, S2).

4. Comparison with Observations

The shorter UKCA models runs listed in Table 3 were used to evaluate mechanism performance against 6 high frequency observational datasets (3 surface/near-surface and 3 aircraft campaigns) from the Amazon, Borneo and the South East USA, all important regions for BVOC production. In addition, satellite-derived isoprene columns (Wells et al., 2020) were compared to model output (Isoprene Column, Table 3). Monthly mean data from the longer CS and CS2 runs (Table 4) for O_3 , CO and $HONO_2$ were also compared to a range of observational data. A summary of the observation datasets is given in Table 5 and locations of the surface and airborne campaigns shown in Fig S3.

Diel profiles for multiple species were calculated from the three surface/near-surface sites and the vertical profiles were calculated from the ATTO site.

The three flight campaigns considered were the October 2005 Amazon GABRIEL campaign (Butler et al., 2008), the July 2008 Borneo Facility for Airborne Atmospheric Measurements (FAAM) (Hewitt et al., 2010) and the Studies of Emissions and Atmospheric Composition, Clouds and Climate Coupling by Regional Surveys (SEAC⁴RS) flight campaign over the South East USA in August - September 2013 (Toon et al., 2016). Hourly model output corresponding to the days and times of the flights was used for the mechanism-observation comparison for each campaign. Model and observational data were binned into 250m/500m altitude bins and median values for the variables of interest across the whole region for a given altitude bin were considered. For the SEAC⁴RS comparison, observational data were also filtered to exclude urban plumes ($NO_2 > 4$ ppb), fire plumes (acetonitrile > 0.2 ppb) and stratospheric air ($O_3/CO > 1.25$) while missing data or data flagged as exceeding the limit of detection were not used and data flagged as a lower limit of detection were set to zero as done in Schwantes et al (2020). Estimated limits of detection are shown for relevant species for the GABRIEL and FAAM campaigns.



The performance of each mechanism is now described for the key species e.g. O_3 , HO_x , isoprene, certain isoprene oxidation products and monoterpenes. A brief commentary about other species including $HONO_2$, CO, PAN, HCHO, MeCHO, EtCHO and acetone is given in the supplement.

4.1 Ozone

CS2 exhibits a modest increase in O_3 (~1-2 ppb) over CS at all surface sites (Fig. 1), exacerbating the existing high surface bias of CS, whose drivers were discussed in Archer-Nicholls et al (2020), and the smaller high bias of ST. On a diel basis, the mechanisms are able to replicate the shape of the diel cycle at the ZF2 site (with similar diel profiles at the ATTO site) but perform less well in Borneo, simulating pronounced diel cycles with a high bias compared to much more muted cycles from observation.

An increase of ~1-4 ppb relative to CS is also exhibited by CS2 for monthly mean O_3 when both mechanisms are compared to observational data at 10 locations from pole to pole at 4 pressure levels (250, 500, 750 and 900 hPa) (Fig. S4). CS2 reduces the low bias in polar regions but increases CS's high bias in the tropics and Eastern US.

Model high biases are also observed from flight data comparisons (Figs. 2(b,f), S6(a)). In the Amazon, where the observed and modelled NO vertical profiles agree well (Fig. S6(e)), there is little difference between the three mechanisms. Each exhibits the greatest high bias at low and a smaller high bias in the free troposphere. CS2 exhibits a high bias of 15-20 ppb for the SEAC⁴RS campaign (Fig. S6(d)), with perhaps some influence from the low altitude NO_2 model high bias. In Borneo, all mechanisms exhibit a roughly consistent high bias of ~20 ppb for ST increasing to 30 ppb for CS2. Interestingly, all the mechanisms simulate a significant low bias for NO_2 (Fig. S6(f)) which may indicate biomass burning events which are not simulated, something which might be expected to promote higher ozone concentrations.

4.2 HO_x

Modelled surface OH increases in all locations from ST through CS to CS2 with a significant increase in midday OH from CS to CS2 (Fig. 1). In Borneo, OH is consistently low biased in the three mechanisms but the best comparison is exhibited by CS2 where the mean diel bias compared to ST and CS decreases by 43-50% and 24-40%, respectively over the period considered. The drivers of the HO_x change are explored further in Section 5.

Surface HO_2 was also simulated to increase in all locations from ST to CS to CS2. Significant high bias was simulated in Borneo (the only observational dataset) (Fig. S7) for the CRI mechanisms, including at night. The simulated ratio of HO_2 to OH is highly biased in all mechanisms. However, it is best simulated in CS2, indicating that the increase in OH is much larger than that for HO_2 . It should be noted that none of the mechanisms at present include the heterogeneous reactions of HO_2 and their inclusion, which will be addressed in future work, should reduce the HO_2 high bias.



The comparison of modelled HO_x to observation is complicated by large discrepancies in key reaction partners. Furthermore, relative to observed values of 100-130 ppb, CO in ST in Borneo is highly biased by 13 ppb and 27 ppb while CO in the CRI mechanisms exhibits larger biases of ~35-50 ppb and ~50-60 ppb during April-May and June-July, respectively (Fig. S7). These high biases would enhance modelled HO_2 at the expense of OH, potentially explaining the modelled low biases in OH. Indeed, the OH model low bias is greater in the June-July period. This highlights the complexity of model-observation comparisons: the CRI mechanisms may well simulate secondary CO production from isoprene more accurately than ST but other model biases, for example in emissions of CO, NO and isoprene, can lead to the CRI mechanisms appearing worse. Nevertheless, if the CO high bias is reduced in future, we might reasonably assume the modelled OH will improve still further.

419

4.3 Isoprene

Modelled isoprene from all three mechanisms was compared to surface observations, flight campaign data and isoprene columns measured by satellite.

423

4.3.1 Isoprene Surface Measurements

CS2 yields the best model-observation comparison for surface isoprene on a daily basis in all locations (Fig. 1 (k-o)). CS2 reduces the high bias in the diel profiles by 50-60% relative to ST and 20-40% to CS at the Z2F, ATTO and Borneo sites, driven by the elevated OH concentrations

428

In most locations the model simulates, to a greater or less extent, a “twin peak” isoprene profile with a sharp rise around 7:00 LT and a second, smaller peak at 19:00 LT. This was most pronounced in the Amazon dry season (ATTO Sept 2013). The morning peak is likely to be due to a combination of the sharp rise in simulated isoprene emissions which starts at 6:00-7:00 am LT, outweighing the concurrent rise in OH, and an underestimation in the model of the rate of BL height growth which can trap isoprene close to the surface, causing a buildup. By contrast, observed isoprene concentrations exhibit a much slower morning growth reaching a peak in early afternoon. While this “out-of-phase” behaviour is unlikely to be the sole driver of model-observation difference, it will play a role since isoprene chemistry occurs on the time scale of ~1-2 hours and atmospheric oxidising capacity varies throughout the day.

437

Over the lowest 80 m at the ATTO site, all mechanisms are high biased in the daytime (9:00-15:00) and nighttime (21:00-3:00) (Fig. S8 (a-d)) with CS2 exhibiting the smallest bias but produce similar isoprene vertical gradients to observations. The effect of boundary layer height was further considered by looking separately at the periods 6:00-8:00 LT and 17:00-19:00 LT (Fig. S8 (e-h)). In contrast to the daytime and nighttime periods, during the 6:00-8:00 period the simulated isoprene gradient is significantly more negative than the observation, indicating less vertical mixing and similar results are seen with the MT profile (Fig. S8 (m-p)). This is most noticeable in September where the largest morning peak is seen in the diel profile for both species and lends support to the theory that the simulated BL height is not increasing as quickly as in reality, leading to more isoprene and MT being trapped at low altitude. Smaller differences between observed and simulated isoprene and MT vertical gradients are seen during 17:00-19:00



LT, coinciding with smaller evening peaks in the diel profiles. This suggests the reduction in BL height is more accurately simulated than the morning increase.

The major drivers of the remaining model-observation difference are likely to be the concentrations of oxidants (despite the increases seen in CS₂, OH remains low biased in Borneo) and the emissions of isoprene (including the modelled vs. actual diel cycle). The concentrations of isoprene and other species also vary significantly through and above the tree canopy, as shown by the ATTO measurements (Fig. S8), and the global model resolution is not high enough to resolve the vertical gradient of species in the canopy. When testing the CRI v2.2 in STOCHEM-CRI with isoprene emissions from the MEGAN-MACC inventory, Khan et al (2021) noted that halving the isoprene emissions reduced the model-observation disagreement significantly and attributed the model high bias in their work to high biases in the emissions of isoprene.

4.3.2 Isoprene Flight Measurements

Model-observation comparisons of isoprene vertical-profiles extending into the boundary layer and into the free troposphere reveal quite a different story from the surface analysis (Fig 2 (a, e, h)).

Despite being high biased at the surface and at low altitude, simulated isoprene vertical profiles over the Amazon and Borneo rapidly show a low bias as latitude increases. There are likely two reasons for this. The first is the vertical mixing, already discussed in relation to the isoprene and MT surface diel cycles. Secondly, for the Amazon and Borneo campaigns only estimated detection limits (0.1 ppb in both cases) could be used. This has the effect of biasing the median of the observational data to higher values as very low values are ignored. In the SEAC⁴RS campaign, all data points flagged as below the detection limit were set to zero, mitigating this issue. The enhanced oxidative capacity of CS₂ at low altitude results in the lowest simulated vertical concentrations among the three mechanisms but the general low bias above the surface is an issue faced by all mechanisms, suggesting it is not just down to modelling of the chemistry.

4.3.3 Isoprene Columns

To consider isoprene on a global scale, monthly modelled isoprene columns for all mechanisms are compared to satellite observations from January, April, July and October 2013 (Wells et al., 2020) (Fig. 3).

Significant variation in model bias is exhibited between the mechanisms with ST exhibiting the highest isoprene columns and CS₂ the lowest. In South America CS₂ exhibits the smallest bias while the ST columns are over double the observed values for April and July. CS and CS₂ exhibit the smallest biases in Africa and Southeast Asia respectively. The low biases in North America ($\sim 0.7\text{--}1.5 \times 10^{15}$ molecules cm⁻²), Europe ($\sim 0.5\text{--}2.7 \times 10^{15}$ molecules cm⁻²) and Central Asia ($\sim 0.1\text{--}1.1 \times 10^{15}$ molecules cm⁻²) are quite consistent across the mechanisms and, in some cases almost equal in magnitude to the observed columns, which suggests the bias is driven more by insufficient emissions rather than the chemistry scheme in these locations.



CS and CS₂ yield lower isoprene columns and generally smaller model biases than ST. This comparison highlights the significant influence of the different chemistry schemes on the simulated isoprene column and thus the considerable challenges of determining isoprene emissions via top-down approaches using back-calculation from observed concentrations or column values: different chemistry schemes will lead to different emission estimates.

4.4 Isoprene Oxidation Products

During the GABRIEL flight campaign, the well-known isoprene oxidation products MACR and MVK were measured via PTRMS and combined as isoprene oxidation products. These species, along with the ISOPOOH, were also measured at the ATTO tower via PTRMS and are compared with model data.

At the ATTO site, all mechanisms are largely high biased but CS₂ produces the best comparison to observations for both diel and vertical profiles (Figs. 1, S9, 11). CS₂ also yields the smallest high bias for the ratio of isoprene oxidation products (isop_{ox}) to isoprene (a metric less sensitive to discrepancies between actual and modelled isoprene emissions) in the Amazon (Figs. 1, S9, 11). Despite the greater oxidising capacity of the PBL in the CS₂ simulations, the isop_{ox} concentrations are lower. This is attributed to the fact that in the relatively low NO_x environment around the ATTO tower, the isomerisation reactions of the isoprene peroxy radical are particularly important and favour the production of HPALDs and other species over MACR, MVK and ISOPOOH.

Relative to the GABRIEL flight data (Fig. 2(d)), the ratio of isop_{ox} to isoprene is high biased in all mechanisms albeit with the CRI mechanisms exhibiting a smaller bias than ST.

4.5 Isoprene Nitrate, IEPOX and HPALDs

The isoprene oxidation products HPALDs and IEPOX, unique to the CS₂ mechanism in this study, are compared, along with isoprene, ISOPOOH and the isoprene nitrate (Fig. S6), to observational data from the SEAC⁴RS campaign over the Southeast USA. Modelled isoprene (Fig 2(h)) exhibits a significant low bias, in line with the isoprene column analysis (Fig. 3) and is attributed to insufficient emissions. Unsurprisingly, ISOPOOH (Fig 2(i)), the isoprene nitrate (Fig. S4(c)) and HPALDs (Fig 2(j)) are also low biased. However, IEPOX (Fig 2(j)) compares favorably to observation.

The apparent good performance of IEPOX, despite the significant low biases of isoprene and its direct precursor ISOPOOH, is likely to be due to a missing sink to the aerosol phase. IEPOX is readily lost to aerosol by reactive uptake (Nguyen et al., 2014, Nguyen et al., 2015, Allan et al., 2014); a process featured in Schwantes et al (2020) (who simulated lower IEPOX concentrations) but not in UKCA. The rate constant for IEPOX's production from ISOPOOH is ~30% lower than that used by a mechanism of similar complexity, MOZART TS2 (Schwantes et al., 2020) while IEPOX's loss via OH has a similar rate constant to MOZART TS2. Including reactive uptake of IEPOX



in future updates may reduce this high bias. The processing of IEPOX is unlikely to affect HO_x-recycling as much as HPALDs, however its importance to SOA formation means it will be a focus of future work.

The low bias of HPALDs, also simulated to a lesser extent in Schwantes et al (2020) who used isoprene emissions from the MEGAN v2.1, is important given its role in HO_x-recycling via photolysis. There remains uncertainty in HPALD photolysis frequencies. In this work simulated HPALD destruction is dominated by reaction with OH and photolysis which are roughly equal ascending to 2.5 km whereupon OH's importance grows rapidly at the expense of photolysis. To test the impact of photolysis uncertainty on the bias, two further runs were performed with the photolysis frequency of HPALDs scaled by 0.5 and 3, respectively. These tests change HPALD concentrations in the lowest 2 km by +30% and -50% (Fig. 2(k), respectively, suggesting concentration of HPALDs is dependent on the photolysis frequency of HPALDs, which is not currently well constrained.

Interestingly, these scaling tests only change low altitude OH by ~2-3% in the south east USA, suggesting the uncertainty in HPALD photolysis from the current approach may not have a huge impact on oxidants in this region although this may in part be due to the modelled isoprene and HPALD low biases (Fig. 2(h,k)). Furthermore, the fact that the modelled photolysis frequency of methacrolein here is low biased by a factor of 2.5-3 (not shown) suggests that, if further changes to the HPALD frequency are made in future, any potential reductions in methacrolein frequency should be scrutinised carefully. Nevertheless, constraining HPALD photolysis further will be a key focus of future work. A lack of OH measurements prevents attempts to constrain the OH loss pathway.

Evaluating HPALD production is also challenging since observations of ISOPO₂ were not measured. Over the relevant temperatures, the rate constant for HPALD production in CS₂ is 6-14 time greater than the equivalent used by Schwantes et al (2020) which would, if anything, make a low bias less likely. The sensitivity of HPALD production to the concentrations of the bimolecular reaction partners of ISOPO₂ (e.g. NO) can also lead to resolution issues with the model: regions with high and low NO concentration treated as a single region within the model (model grids can be up to ~125 km wide at the equator) with moderate [NO], suppressing HPALD formation (see Schwantes et al., 2020). A commentary on the global distribution of HPALDs and IEPOX is given in Section 5.

4.6 Monoterpenes (MT)

Simulated surface diel monoterpene profiles (Fig. 1) are characterised by early morning and evening peaks which are not present in observations. As discussed in relation to the isoprene diel cycle, the morning peak is probably caused by a combination of the simulated emissions increasing too early and a delayed evolution of the simulated BL height, trapping large quantities of monoterpenes close to the surface (Fig. S8). The evening peak coincides with a reduction of simulated OH to near zero and therefore is probably driven by oxidant reduction as well as a reduction in the BL height. Around midday the mechanisms do a better job in most locations with the lower values in the CRI mechanisms driven by the greater oxidant concentrations. In 4 of the 5 locations, CS₂ yields the smallest model bias although it is acknowledged that other issues, such as the BL dynamics, need attention.



5. Comparison to CRI-STRAT

The performance of the CS mechanism to the simpler ST mechanism was discussed in detail in Archer-Nicholls et al (2020). Here we describe chemical composition of the atmosphere simulated by CS2 relative to that from CS using the longer model runs summarised in Table 2. Particular attention is paid to O_3 and its production and loss fluxes, HO_x , isoprene and monoterpenes, the isoprene oxidation productions IEPOX and HPALDs, nitrated species (NO_y) and the potential impacts to aerosols. Changes to CO and HCHO are discussed in the SI Section S5.

5.1 O_x

As in Archer-Nicholls et al (2020), the change to O_3 was analysed by considering the sum of odd oxygen, NO_2 and its reservoir species, termed O_x , and defined in Eq. (1).

$$O_x = O + O_3 + NO_2 + 2N_2O_5 + 3NO_3 + HONO_2 + HO_2NO_2 + PANs \quad (1)$$

Tropospheric O_3 burden increases by 8% from 328 Tg in CS to 354 Tg in CS2. Much of the free troposphere exhibits increases of 2-6 ppb (~6-14%) in O_3 with large parts of the tropical troposphere increasing by more than 4 ppb (Fig. 1). This increase is driven chiefly by a 1.3% decrease in O_x chemical destruction, resulting in an 12% increase in net chemical O_x production. The sensitivity tests (Table S3) reveal the update to the isoprene mechanism only has a minor effect on O_3 burden (~2 Tg decrease) while the changes to $O(^1D)$ and inorganic nitrogen reactions each yield increases of 17 Tg (when considered in isolation) with greater impacts in the lower and upper troposphere, respectively (Fig. S16). The changes to the O_3 burden in the sensitivity tests do not sum to the total 26 Tg increase from CS to CS2 which indicates a degree of interplay between the different updates, an unsurprising result given ozone's central role in tropospheric chemistry.

O_x lifetime, defined as the ratio of O_x burden (B_{O_x}) to the sum of chemical (L_{O_x}) and physical (D_{O_x}) O_x loss fluxes (Eq. 2) (Young et al., 2018, Archibald et al., 2020b), increase by 8% equivalent to 18.8 days in CS2, while ozone production efficiency (OPE), defined as moles of O_x produced (P_{O_x}) per mole of NO_x emitted (E_{NO}) (Eq.3) (Archer-Nicholls et al., 2020) increases negligibly from 33.74 to 33.78.

$$\tau_{O_x} = \frac{B_{O_x}}{L_{O_x} + D_{O_x}} \quad (2)$$

$$OPE = \frac{P_{O_x}}{E_{NO}} \quad (3)$$

O_3 below 500 m increases across almost the entire globe with increases of 2-4 ppb (~5-7.5%) over much of Europe, Africa and the Americas and 4-5 ppb over India and China (Fig. 4), exacerbating the existing high bias in CS (Archer-



Nicholls et al., 2020). The sensitivity tests allow this change to be partially decomposed into the different drivers (Fig. S13). The update to isoprene chemistry produces localised increases in O_3 over the tropical forested regions of South America, Africa and East Asia of 2–4 ppb: the increase in O_x production via $HO_2 + NO$ and $MeO_2 + NO$ outweigh the reduction in the non-methyl peroxy radicals ($RO_2 + NO$) pathway (discussed later). While comparison to Khan et al (2021) is difficult given the multiple mechanistic differences, O_x production from $RO_2 + NO$ also decreased in their study. The changes to $O(^1D)$ also yield an increase in >1 ppb across the entire globe (due to reduced O_x loss via $O(^1D) + H_2O$) with a larger increase (2–3 ppb) encompassing ~20S–40N. The change to inorganic nitrogen also leads to terrestrial increases of 2–4 ppb from increased O_x production via $HO_2 + NO$ and $RO_2 + NO$.

5.1.1. O_x Budget

O_x production and loss fluxes for CS and CS2 are given in Table 6 and the breakdown for the sensitivity tests is given in Table S3. O_x production decreases in CS2 in much of the tropical and SH BL and lower free troposphere but increases in the NH midlatitude BL and tropical high troposphere while O_x loss decreases strongly in the tropical BL and lower free troposphere (Fig. 5). Despite the modest changes to total O_x production and loss fluxes, the story is more complicated than it first appears due to offsetting changes to the key chemical production and loss fluxes.

5.1.2 O_x production

The $HO_2 + NO$ pathway represents the largest absolute increase of O_x production (3.2%, Table 6) with particular increases in the NH tropics and mid latitude boundary layer and tropical upper troposphere (Fig. S12). The drivers of this change are complex: the low altitude increases are driven by the significant increases in HO_2 (Fig. 6), which exceed 5% in places, while at higher altitude the increase is attributed to a localised 15–20% rise in NO . The sensitivity tests suggest the change to the isoprene scheme (CS2_isoprene) is a key driver in the rise of low altitude HO_2 (and thus the flux) while the change to the inorganic nitrogen reactions (CS2_inorgN) also contribute to the increased flux at low altitudes and are chiefly responsible for the increase at higher altitudes.

However, the increase in $HO_2 + NO$ is offset by a decrease in the $NO + RO_2$ flux (15.4%, Table 6) where RO_2 comprises all peroxy radicals except the methyl peroxy radical, MeO_2 . This reduction is strongest in the tropical BL and low free troposphere and driven by a significant decrease in the RO_2 burden (32%). This burden reduction arises from the isomerisation pathways which inhibit the conversion of the isoprene-derived peroxy radical, $RU14O_2$, to the other peroxy radicals $RU12O_2$ and $RU10O_2$ (via reactions with standard partners such as NO and NO_3) by providing competing routes which yield other species whose degradation pathways do not produce further RO_2 (Khan et al., 2021). For example, the HPALDs produced are photolysed to hydroxy acetone and unsaturated hydroxy carbonyls which further degrade producing mostly closed-shell products and HO_2 . This rapid reaction pathway for $RU14O_2$ sees its burden decrease by 35% in CS2 compared to CS and tropical low altitude mixing ratios decline by over 30%. Similar declines in the $RO_2 + NO$ flux (15%) and RO_2 burden (33%) are seen for CS2 relative to the CS2_isoprene sensitivity test, providing strong evidence that the change to isoprene is driving the change in RO_2 . Khan et al (2021)



also simulated a reduction in RO₂ burden (and a corresponding drop in O₃ production via this pathway) although their decrease of 6.5% is less than half the equivalent value (including MeO₂) of 15% in this work, likely due to the other differences between the mechanisms used in their work and this study (see Section 1).

The fluxes of NO with HO₂, MeO₂ and RO₂ account for over 99.5% of total O_x production in both mechanisms and the changes in other pathways are an order of magnitude smaller in absolute terms. The reduction in the rate constant for OH + MeONO₂ (Section 4.1) reduces O_x production from organic nitrate oxidation significantly while also driving the increase in O_x production from organic nitrate photolysis. The addition of the photolysis of isoprene hydroxy nitrate and the other nitrates RU12NO₃ and RU10NO₃ make smaller contributions.

5.1.3 O_x loss

The change in O_x chemical destruction is dominated by the reduction in O(¹D) + H₂O reaction (7.2%) which accounts for 54% of O_x loss in CS but only 49% in CS2. In the sensitivity run CS2_O1D, which uses the same O(¹D) rate constants as CS, the O(¹D)+H₂O flux accounts for 54% of O_x chemical loss. As this reaction involves water, the change is strongest in the tropical BL and low free troposphere (Fig. S14).

The increase in O_x loss via HO₂ + O₃ (9.1%, Table 6) is driven predominantly by changes to the inorganic nitrogen and O(¹D) reactions while the isoprene scheme is simulated to have little impact. O_x loss via OH + O₃ also increases (7.6%) despite the decrease in free troposphere HO_x with the new isoprene chemistry and revised inorganic nitrogen reactions simulated to play important roles. O_x destruction from O₃ + alkene reactions decline significantly (39%) yet increase at very low altitudes (<500 m) before decreasing at higher altitudes. This altitude dependence may arise from the enhanced O₃ low altitude driving a greater O₃ + alkene flux but, at higher altitudes, the depletion of the VOCs by O₃ and the elevated OH, means O₃ destruction is lower.

5.2 HO_x

The change to OH shows significant spatial and altitudinal variation, increasing at low altitude over land but decreasing over the oceans and in much of the free troposphere. This stems from the different drivers of OH concentrations and their relative importance in different regions.

At low altitude, the terrestrial increases in OH (Fig. 6(c,d)) are revealed by the sensitivity tests to be driven predominantly by the isoprene scheme: a clear illustration of impact of the HO_x-recycling chemistry (Fig. S15). The inorganic nitrogen changes make a smaller contribution to the low latitude OH increase while the O(¹D) changes reduce low altitude OH but this effect is only noticeable over the oceans.

This significant increase in low terrestrial altitude OH is of particular interest in the context of BVOCs and their impact on the chemical composition of the atmosphere. Concentrations in the lowest 500 m increase by $2\text{--}3 \times 10^5 \text{ cm}^{-3}$ (30–50%) in much of the Amazon with similar changes seen in other tropical regions and the Southeast USA; regions with the greatest emissions of isoprene and BVOCs. The boreal forest regions in North America and Eurasia exhibit modest



increases of up to 10% in places since isoprene emissions are lower (Fig. S15). The influence of the updated isoprene chemistry is further apparent when the HO_x production flux from two of the key new HO_x -recycling pathways - photolysis of the HPALD and hydroxy unsaturated carbonyl (HUCARB9) species - is compared to that from $\text{O}(^1\text{D}) + \text{H}_2\text{O}$ (Fig. 6f). Over the Amazon and other tropical regions, HO_x flux from this pathway amounts to 20-40% of that from $\text{O}(^1\text{D}) + \text{H}_2\text{O}$. The difference in BVOC-driven depletion of oxidant concentrations at low altitudes will be even more pronounced when CS_2 is compared with ST which exhibited even lower tropical low altitude HO_x (e.g. Fig. 9, Archer-Nicholls et al., 2020).

However, in much of the free troposphere, OH decreases by 2-10% relative to CS due to the changes made to the $\text{O}(^1\text{D})$ rate constants (Fig. S20) which reduces the fraction of $\text{O}(^1\text{D})$ reacting with H_2O (Fig. 6(a)). This general decline is reversed in the upper tropical troposphere (10-15 km) where OH increases by up to 15%, driven by an increase in NO stemming from the update to inorganic nitrogen reactions and a smaller contribution from the updated isoprene chemistry (Fig. S16). These free troposphere changes partially reverse the changes simulated between CS and ST (Fig. 6, Archer-Nicholls et al., 2020). In that comparison, tropical free troposphere OH (~2-6 km) increased in CS relative to ST by $0.5\text{--}2 \times 10^5 \text{ cm}^{-3}$ while here CS_2 yields a decrease in the same location of $0.25\text{--}1 \times 10^5 \text{ cm}^{-3}$ compared to CS. In the upper tropical troposphere, CS decreased OH by $1\text{--}4 \times 10^5 \text{ cm}^{-3}$ relative to ST while CS_2 exhibits an increase of $0.25\text{--}1.5 \times 10^5 \text{ cm}^{-3}$ in the same region compared to CS. Thus, the distribution of free troposphere OH in CS_2 is more similar to that in ST than the CS distribution is.

Overall, the reduction in the free troposphere OH outweighs the increases elsewhere with the tropospheric air mass-weighted concentration and burden of OH decreasing in CS_2 by 1.5% and 0.49% respectively. This is in sharp contrast to the 6.4% increase in burden simulated by Khan et al (2021). However, in the $\text{CS}_2\text{_{O1D}}$ sensitivity test the OH burden increases by 6.6 % relative to CS allowing us to be confident that this discrepancy between Khan et al (2021) and this work is down predominantly to the differing $\text{O}(^1\text{D})$ rate constants. Despite the increase in surface OH, the net reduction in tropospheric OH yields a 2.3% increase in methane lifetime from 7.43 to 7.60 years (Table 7), also in contrast to the 0.5 years decrease in methane lifetime simulated by Khan et al (2021). However, the isolated change to isoprene chemistry, given by the comparison of CS_2 and $\text{CS}_2\text{_{isoprene}}$, causes a methane lifetime decreases of 2.2% due to the enhanced low altitude OH.

HO_2 also increases at low altitude (up to 6-8% at the surface, Fig. 6(b)), driven primarily by the new isoprene chemistry, yet this increase extends much further into the free troposphere than OH, reaching nearly 5 km above the equator. HO_2 decreases in the rest of the free troposphere, partially from $\text{O}(^1\text{D})$ changes, and does not exhibit the high increase shown by OH, rather declining by 6-8% in the tropical high troposphere resulting in a burden decrease of 0.7%. The greater increase in low altitude HO_2 (than for OH) is likely to be due in part to co-located increases in CO of 3-6 ppb (see SI and Fig. S21(a)).

5.3 BVOCs



The interactive nature of iBVOC emissions led to average isoprene emissions being 0.36 Tg yr^{-1} (0.06%) lower in CS2 while monoterpene emissions were 0.05 Tg yr^{-1} (0.05%) lower. However, these differences are dwarfed by the reductions in the burdens of isoprene, α -pinene and β -pinene of 26%, 18% and 15%, respectively.

Isoprene mixing ratios averaged over the lowest $\sim 100\text{m}$ decrease by 1-3 ppb ($\sim 10\text{-}30\%$) in large parts of South America, Africa and South East Asia (Fig. 7). The greater terrestrial low altitude HO_x increases the OH-initiated oxidative flux of isoprene by 3.5 %, attributable almost entirely to the updated isoprene scheme. However, this is actually outweighed by a 23% decrease in isoprene destruction by O_3 while oxidation via NO_3 increased by 3.7%. Despite the modest global increase, isoprene oxidation is confined even more to low altitude regions (Fig. 7), a feature also simulated by Karset et al (2018) (Fig. 8). This also results in lower mixing ratios throughout the whole troposphere (Fig. 7).

α -pinene's chemical destruction by OH, O_3 and NO_3 changed by 7.5%, -6.3% and -0.8% respectively leading to a total flux increase of 0.05 Tg yr^{-1} (+0.05%). The corresponding changes for β -pinene with OH, O_3 and NO_3 were 7.6%, 5.8% and 12.9% with a total increase of 3.59 Tg yr^{-1} (+7.9%).

The reductions to these BVOC burdens are greater than those simulated by Khan et al (2021) of 17%, 4% and 9% for isoprene, α -pinene's and β -pinene respectively. However, Khan et al (2021) simulated a reduction in O_3 over tropical regions and a much smaller increase in NO_3 burden (1%) which would have resulted in significantly lower BVOC destruction fluxes, particularly for the monoterpenes. As discussed in Section 4, CS2 simulates a reduction in the model high bias of surface isoprene and, to a lesser extent, monoterpenes, compared to CS and ST.

5.4 HPALDs and IEPOX

While a comparison cannot be made between CS and CS2 for HPALDs and IEPOX, their importance for HO_x -recycling and SOA formation respectively means examining their global distribution is still useful. Both species follow the surface distribution of isoprene closely (Fig. 8) with IEPOX concentrations typically an order of magnitude greater than HPALDs, something also reflected in their burdens (0.39 Tg and 0.02 Tg , respectively). As discussed in Section 4, loss of IEPOX to aerosol via reactive uptake is not currently modelled and simulated concentrations will decrease once this process is included. Indeed, accurate modelling of IEPOX and its contribution to SOA has been suggested to be important in future climate scenarios (Jo et al., 2021) which highlights the benefits of including IEPOX in CS2 but also the need for careful consideration of how aerosol uptake is modelled. Simulated advection up to the upper tropical troposphere is clearly seen in the DJF zonal means with potentially important consequences for IEPOX-derived SOA which has been observed in the lower troposphere in flight campaigns (e.g. Allan et al., 2014).

5.5 NO_y



The distribution of nitrated products (NO_y) between reactive (NO_x) and reservoir species (NO_z) changes between CS and CS2 and is detailed in Table 8. Here we use the standard definitions of NO_x , NO_z and NO_y (Archer-Nicholls et al., 2020) (Eq. 4,5,6):

$$\text{NO}_x = \text{NO} + \text{NO}_2 \quad (4)$$

$$\text{NO}_z = \text{NO}_3 + 2\text{N}_2\text{O}_5 + \text{HONO}_2 + \text{HO}_2\text{NO}_2 + \text{ClONO}_2 + \text{BrONO}_2 + \text{PANs} + \text{RONO}_2 + \text{CH}_3\text{O}_2\text{NO}_2 + \text{Nitrophenols} \quad (5)$$

$$\text{NO}_y = \text{NO}_x + \text{NO}_z \quad (6)$$

(RONO_2 comprises alkyl nitrates, hydroxy nitrates and hydroperoxy nitrates while PANs comprises all species with the peroxy acetyl nitrate functionality).

The NO_y burden decreases by 4.8% (in terms of mass of N), driven primarily by a 20% decline in PANs. However, the NO_x burden increases by 4% with the widespread increase in the tropical high troposphere of 10-20 ppt (up to 25%) outweighing the reduction in the NH midlatitude PBL (10-50 ppt, 1-2.5%) (Fig. 9(a)). The increase in NO_x and the reduction in NO_y leads to the fraction of NO_y as reactive Nitrogen increasing by 9% and the associated increases to the O_3 production, particularly in the free troposphere, are identified in Section 5.1. The sensitivity tests revealed the high-altitude NO_x rise to be driven predominantly by the change to the inorganic nitrogen with a smaller contribution from the updated isoprene scheme (Fig. S17).

The 6% reduction in NO_z burden is dominated by the decrease in PANs which exceeds 40 ppt in most of the 40N-40S troposphere (Fig. 10(e)). The decrease in the PANs formation rate constant discussed in Section 2 is not the principal driver of this reduction despite reducing by 40% in much of the troposphere. For the single year used for the sensitivity tests, the PANs burden in CS2_inorgN (featuring the larger formation rate constant) (0.292 TgN) is much closer to that in CS2 (0.290 TgN) than in CS (0.364 TgN). A more important factor is the reduction in the PAN-precursor acyl peroxy radical (MeCO_3), driven by the updated isoprene chemistry, whose burden decreases by over 20% in both CS2 and the sensitivity test CS2_inorgN. This dependency is clearly illustrated by the fact that the isolated change to the inorganic nitrogen reactions (CS2_inorgN) only produces a small decrease to low altitude PANs while the change to isoprene scheme (CS2_isoprene) yields a much larger decrease in PANs in spatial agreement with the CS2-CS difference (Fig. S18). The PANs burden of 0.317 TgN in the CS2_isoprene test is also closer to that in CS. However, the change in PANs between CS2 and CS is still larger than that simulated from the isolated isoprene chemistry change alone which suggests there are some synergistic effects occurring.

The 0.4% increase in HONO_2 , including increases of up to 30 ppt in the tropical mid troposphere (Fig. 9(d)), is driven more by the update to the isoprene scheme than the change to inorganic nitrogen reactions (Fig. S19).



The 59% increase in RONO₂ burden in CS2 is predominantly due to the significant reduction in the rate constant for the OH-initiated destruction of MeONO₂, the principal organonitrate, which brings CS2 into agreement with STRAT-TROP and the most recent IUPAC value. At 290 K, the rate constant is 18 times lower in CS2 and at 250 K 50 times lower, yielding a 3-fold MeONO₂ burden increase. The update to the isoprene scheme, when isolated, actually reduces RONO₂, despite the introduction of the two new organic nitrates (RU12NO₃ and RU10NO₃). As discussed in the context of the RO₂ burden, this is driven by the added competition from the RU14O₂ isomerisation reactions: the flux of the RU14O₂ + NO reaction is 15% lower in CS2 than CS. The increase in RONO₂ is simulated to be 10-20 ppt in the tropical lower altitude and 2-10 ppt for the rest of the troposphere (Fig. 9(f), S20).

With the significant drop in PANs as a fraction of NO_y (34% to 28%) and the increase in HONO₂ and NO_x, the breakdown of NO_y in CS2 is closer to that in ST (Archer-Nicholls et al., 2020). The increase in RONO₂ is the only major exception to this since ST, which only has two organonitrate species (isoprene nitrate and MeONO₂), has a lower RONO₂ burden than CS.

5.6 Impacts on Aerosols

A key area of future research with the CRI mechanisms will be on their influence on aerosols. The spatial changes to oxidants are also likely to influence secondary organic aerosol (SOA) formation, as discussed in Section 1. In UKCA, SOA is produced from the tracer Sec_Org, a surrogate for the oxidised products of α -pinene and β -pinene which adds to existing organic aerosol with an optional boundary layer nucleation scheme involving Sec_Org and H₂SO₄ based on Metzger et al (2010) also available. The Sec_Org burden decreases by 7% in CS2 with noticeable annual variation (DJF -10%, JJA -4%). Despite the burden decrease, within the lowest 500m in the tropics Sec_Org mass concentration increases by 2-10%, driven by an increase its production from α -pinene and β -pinene (Fig. 10(a,b)). Above this region, Sec_Org production and mass concentration decrease and so it appears the greater low altitude oxidative capacity in CS2 leads to greater production of Sec_Org within the boundary layer but lower concentrations above it. This is likely to have an impact on SOA distribution (and lifetime) since deposition and loss to the aerosol phase is greater in the boundary layer due to the steep decline in aerosol surface aerosol density with altitude. Further detailed analysis involving the fluxes of Sec_Org to aerosol and the resulting changes to size and number distributions are beyond the scope of this work but examining wider consequences for SOA, in the context of the BVOC-mediated feedback between the biosphere and climate, will form a key area of future research. It is also worth noting an even more pronounced perturbation to SOA may be seen if isoprene is allowed to produce Sec_Org which is a more realistic approach to simulating SOA (e.g. Scott et al., 2015) and will be explored in future work.

The global perturbation to the oxidation pathways of SO₂, another important aerosol precursor, are more modest. From CS to CS2, the oxidative fluxes of SO₂ with OH, H₂O₂ and O₃ change by +0.9%, +0.02% and 1.7%, respectively while the tropospheric sulphate aerosol burden decreases by just 2.3%. However, as with isoprene oxidation and Sec_Org production, the burden change belies the more complex perturbations occurring. The increased oxidants at lower altitude and reduction at greater altitudes result in gas phase SO₂ oxidation increasing by 2.5-10% in the tropical and



midlatitude PBL yet decreasing at higher altitudes (Fig. 10(c,d)). This effect is expected to be even more pronounced when CS2 is compared to ST which simulates even lower low altitude OH than CS (Archer-Nicholls et al., 2020) and has been the standard mechanism for investigations into aerosol-oxidant coupling in UKCA (Thornhill et al., 2020, Weber et al., 2020, O'Connor et al., 2020). Therefore, the mechanism-driven changes to oxidants are likely to have consequences for both SOA and sulphate aerosol. While a full investigation into oxidant aerosol coupling is beyond the scope of this paper, it will form a central part of future work with the CRI mechanisms.

5.7 Summary and synthesis

The key changes between CS and CS2, driven by the multiple chemistry changes, can be summarised as follows:

1. O_x production increases marginally in CS2 but a larger decrease in O_x destruction, driven by a significant reduction in the $O(^1D) + H_2O$ flux, leads to a greater O_3 tropospheric burden and mixing ratios.
2. The update to the isoprene chemistry increases low altitude tropical HO_x but the reduction in OH production from $O(^1D) + H_2O$ results in lower HO_x concentrations in much of the free troposphere, increasing methane lifetime.
3. The update to the inorganic nitrogen reactions increases NO_x as a fraction of NO_y with a significant increase in the upper tropical free troposphere and a co-located increase in OH. The PAN burden decreases by 20%.
4. The increase in boundary layer oxidative capacity reduces the burden of BVOCs and confines their oxidation even more to low altitude with likely consequences for aerosol production and lifetime.

6. Conclusion

The radiative impact of isoprene, via its influence on atmospheric chemical composition and organic aerosol, means an accurate description of its chemical behaviour is crucial for advancing our understanding of pre-industrial, present day and future atmospheres. In this study we describe the incorporation of the Common Representative Intermediates chemistry scheme version 2.2 (CRI v2.2), along with accompanying stratospheric chemistry, into the global chemistry-climate model UKCA to create the mechanism CRI-Strat 2 (CS2). The introduction of CS2 into UKCA facilitates a semi-explicit description of HO_x -recycling chemistry during isoprene oxidation via the isomerisation of isoprene peroxy radicals to produce HPALDs which yield HO_x upon photolysis. This is a key process for reconciling the model low bias of HO_x in low NO_x , BVOC-rich regions. In addition, CS2 also features updates to the rate constants of the reactions of $O(^1D)$, inorganic nitrogen and organic peroxy radicals with NO and NO_3 , bringing the mechanism into agreement with the most recent IUPAC values. CS2 is one of the first mechanisms with this functionality suitable for long term climate integrations.

A rigorous comparison using UKCA with CS2 and two other chemical mechanisms, STRAT-TROP (ST) (the standard chemistry mechanism used in UKESM1's contributions to CMIP6 experiments) and CRI-STRAT (CS) (which has tropospheric chemistry from an earlier version of the CRI, CRI v2.1), is performed against high frequency surface and airborne observational data from BVOC-rich regions for multiple chemical species including O_3 , OH, HO_2 , isoprene and monoterpenes and isoprene oxidation production. The HO_x -recycling in CS2 results in significantly enhanced



861 surface diel OH (up to 50% higher than CS at midday) in the Amazon and Borneo (improving model low bias), leading
 862 to improved modelling of diel and vertical isoprene profiles and reducing the mean 24-hour bias by 50-60% and 20-
 863 40% relative to ST and CS, respectively across the locations considered. However, CRI-Strat 2 exacerbates the existing
 864 isoprene model low bias away from the surface, suggesting potential issues with model vertical convection. CS and
 865 CS2 yield smaller isoprene column biases compared to observations than ST, in line with the surface and free
 866 troposphere observational comparisons, while also illustrating the significant influence the chemical mechanism has
 867 on modelled column. This comparison also highlights the significant influence the different chemistry schemes have
 868 on the simulated isoprene column and thus the considerable challenges of determining isoprene emissions via back-
 869 calculation.

870

871 The low altitude high biases for O₃ in CS increase modestly (1-2 ppb) in CS2. Simulated monoterpene concentrations
 872 are high biased at the surface at most of the locations considered with CS2 returning the smallest bias. As with
 873 isoprene, simulated monoterpenes display sharp morning and evening peaks which are believed to be due to boundary
 874 layer height issues. Model high bias of IEPOX and the low bias of HPALDS suggests further investigation of the key
 875 processes of loss to aerosol for IEPOX and HPALD photolysis frequency are needed.

876

877 In addition to observational comparisons, a detailed comparison of UKCA model output using CS2 is performed,
 878 complementing the earlier comparison of ST and CS (Archer-Nicholls et al., 2020). Sensitivity tests are also performed
 879 to help isolate the drivers of the differences between CS and CS2. CS2 simulates an 8% increase in tropospheric O₃
 880 burden driven primarily by reduced O_x loss as the changes to rate constants of O(¹D) with H₂O, O₂ and N₂ mean that
 881 a smaller fraction of O(¹D) reacts with H₂O to produce OH. Low altitude O₃ increased by 2-4 ppb over much of the
 882 globe, driven predominantly by changes to the O(¹D) and inorganic nitrogen reactions. More broadly, the widespread
 883 influence of the changes the rate constants of O(¹D) and multiple inorganic nitrogen species highlights the importance
 884 of having accurate information for these parameters.

885

886 Relative to CS, low altitude OH increased over terrestrial regions, exceeding 50% in some tropical forested regions,
 887 primarily due to the influence of HO_x-recycling from isoprene. However, OH decreased over the oceans and in much
 888 of the free troposphere driven by updates to the rate constants of O(¹D)'s reactions with H₂O, O₂ and N₂. As a result,
 889 methane lifetime increased by 1.9%, in stark contrast to previous studies using CRI v2.2 in the STOCHEM model
 890 which did not make changes to O(¹D) and inorganic nitrogen reactions. When the changes to isoprene chemistry were
 891 isolated, methane lifetime decreased by 2.2%, qualitatively in line with previous studies. The addition of isomerisation
 892 pathways in the updated isoprene scheme reduced the methyl (7%) and non-methyl peroxy (36%) radical burdens.

893

894 The distribution of nitrated species (NO_y) in CS2 was closer to that simulated in ST than CS with a significant
 895 reduction (20%) in the burden of PANs which was driven by a reduction in the precursor RO₂. The NO_x burden
 896 increased by 4%.

897



898 The increase in low altitude OH reduced the burdens of isoprene (25%) and monoterpenes (11-18%) and the extent of
 899 their dispersion: more oxidation took place in the boundary layer where loss of oxidation products such as the lumped
 900 SOA precursor Sec_Org to existing aerosol is likely to be greater. Enhanced SO₂ oxidation in the boundary layer was
 901 also simulated. These changes are likely to have implications for SOA and sulphate aerosol, particularly as CS has
 902 already been shown to have a more highly oxidising boundary layer than ST. Therefore, the difference between CS2
 903 and ST (the mechanism used to explore chemical-aerosol coupling in UKESM1 in CMIP6 experiments), is likely to
 904 be significant and will be the subject of future work.

905
 906 The addition of CS2 also lays the groundwork for the incorporation of a novel chemistry scheme which describes the
 907 formation of the highly oxidised organic molecules (HOMs) derived from biogenic species such as α -pinene (e.g.
 908 CRI-HOM, Weber et al., 2020b). HOMs are crucial for new particle formation without sulphuric acid (Kirkby et al.,
 909 2016, Simon et al., 2020), a process which is an important source of new particles in the Amazonian free troposphere
 910 (Zhao et al., 2020) and has been simulated to have consequences for our understanding of pre-industrial aerosol burden
 911 (Gordon et al., 2016). The influence of isoprene in HOM production (Kiendler-Schaar et al., 2009, McFiggans et al.,
 912 2019, Heinritzi et al., 2020) can also be captured by addition of CRI-HOM making UKCA one of the very first global
 913 chemistry-climate models to feature a semi-explicit representation of HOMs and enabling further investigation into
 914 the climatic impact of the interaction between BVOCS. Long chain terpenes addition to CS2 are also planned including
 915 sesquiterpenes, which may reduce the surface ozone high bias and form HOMs, and improvements to the uptake of
 916 oxidised species to plant surfaces.

917
 918 While certain elements of the CRI-STRAT 2 mechanism in UKCA such as the ozone high bias remain problematic,
 919 its incorporation represents a major step forward in our ability to simulate isoprene chemistry in low NO_x
 920 environments. The simulated changes to oxidants in CRI-Strat 2 will affect the atmosphere's radiative balance by
 921 perturbing certain greenhouse gases and aerosols and investigating the impact will be a major topic of future work. In
 922 particular, the feedback between the biosphere and climate, mediated by BVOCS, will be evaluated using multiple
 923 mechanisms to assess their influence. CRI-Strat 2 can be taken up for use, alongside other mechanisms, to further our
 924 understanding of the wide-ranging impact BVOCS have on climate.

925
 926
 927 *Data Availability:*

928
 929 The description of the Z2F field campaign is given SI Section S4 and the observational data is available at
 930 <https://doi.org/10.17863/CAM.65133>

931
 932 The observational data from the SEAC4RS flight campaign is available at [https://www-air.larc.nasa.gov/cgi-](https://www-air.larc.nasa.gov/cgi-bin/ArcView/seac4rs?MERGE=1#60_SECOND.DC8_MRG/)
 933 [bin/ArcView/seac4rs?MERGE=1#60_SECOND.DC8_MRG/](https://www-air.larc.nasa.gov/cgi-bin/ArcView/seac4rs?MERGE=1#60_SECOND.DC8_MRG/).

934



The observational data from the ATTO tower is available to download at <https://www.attodata.org>. Specific datasets used were <https://www.attodata.org/ddm/data/Showdata/72>, <https://www.attodata.org/ddm/data/Showdata/73>, <https://www.attodata.org/ddm/data/Showdata/74> and <https://www.attodata.org/ddm/data/Showdata/77>.

The observational data from the FAAM aircraft is available at <http://data.ceda.ac.uk/badc/op3/data/op3-aircraft> and Borneo data can be found at <http://data.ceda.ac.uk/badc/op3/data>.

Data tables of the full CRI-Strat 2 mechanism and the mechanisms used in the sensitivity test described in this paper are included in the supplement. The CRI v2.2 mechanism can be viewed and downloaded from <http://cri.york.ac.uk>.

Model data and analysis code is available from JW on request.

Code Availability

Due to intellectual property right restrictions, we cannot provide either the source code or documentation papers for the UM. The Met Office Unified Model is available for use under licence. A number of research organisations and national meteorological services use the UM in collaboration with the UK Met Office to undertake basic atmospheric process research, produce forecasts, develop the UM code and build and evaluate Earth system models. For further information on how to apply for a licence; see <https://www.metoffice.gov.uk/research/approach/modelling-systems/unified-model> (last access: 24 November 2020).

Author Contributions

Mechanism incorporation was carried out by JW, SAN and NLA with advice from ATA, YMS, MJ, MAHK and DES. Observational comparison experiments were designed by JW, SAN, NLA and ATA and executed by JW, mechanism-mechanism comparison experiments were designed by JW, ATA, NLA and SAN and executed by JW. TJB, CJP, AB and PA compiled and supplied the Z2F Brazil observational data and TJB wrote the field campaign description in the SI, RS advised on the SEAC⁴RS data and analysis, JW, SAN, ATA, JW* interpreted the Z2F Brazil, Borneo, ATTO, FAAM, GABRIEL and SEAC⁴RS observational data. JW wrote the paper. All co-authors discussed the results and commented on the paper.

(JW = James Weber, JW* = Jonathan Williams)

Competing interests.

The authors declare that they have no conflict of interest.

Financial support.

JMW has been funded by a Vice-Chancellor's Award from the Cambridge Trust. SAN and ATA have been funded by NERC PROMOTE (grant no. NE/P016383/1). NLA and ATA are supported by NERC and NCAS through the



973 ACSIS project. YMS has been funded by NERC through the University of Cambridge ESS-DTP. MAHK and DES
 974 are funded by NERC (grant code-[NE/K004905/1](#)), Bristol ChemLabS and the Primary Science Teaching Trust. TB,
 975 CJP, AB and PA acknowledge funding from FAPESP – Fundação de Amparo à Pesquisa do Estado de São Paulo,
 976 grant number 2017/17047-0.

977

978 *Acknowledgements*

979 This work used Monsoon2, a collaborative High Performance Computing facility funded by the Met Office and the
 980 Natural Environment Research Council. This work used JASMIN, the UK collaborative data analysis facility.

981

982 We are grateful to Dr Horst Fischer, Dr Hartwig Harder, Dr Pete Edwards for their assistance and advice and to
 983 Professor Jason Surratt for providing the calibration standards for the Z2F Brazil study. We thank the field support
 984 from the LBA central office at INPA in Manaus.

985

986 *References*

987

988 Abraham, N.L., Archibald, A.T., Cresswell, P., Cusworth, S., Dalvi, M., Matthews, D., Wardle, S. and Whitehouse,
 989 S., 2018. Using a virtual machine environment for developing, testing, and training for the UM-UKCA composition-
 990 climate model, using Unified Model version 10.9 and above. *Geoscientific Model Development*, 11(9), pp.3647-3657.

991

992 Allan, J.D., Morgan, W.T., Darbyshire, E., Flynn, M.J., Williams, P.I., Oram, D.E., Artaxo, P., Brito, J., Lee, J.D. and
 993 Coe, H., 2014. Airborne observations of IEPOX-derived isoprene SOA in the Amazon during SAMBBA. *Atmospheric*
 994 *Chemistry and Physics*, 14(20), pp.11393-11407.

995

996 Archibald, A.T., Levine, J.G., Abraham, N.L., Cooke, M.C., Edwards, P.M., Heard, D.E., Jenkin, M.E., Karunaharan,
 997 A., Pike, R.C., Monks, P.S. and Shallcross, D.E., 2011. Impacts of HO_x regeneration and recycling in the oxidation
 998 of isoprene: Consequences for the composition of past, present and future atmospheres. *Geophysical Research Letters*,
 999 38(5).

1000

1001 Archibald, A.T., O'Connor, F.M., Abraham, N.L., Archer-Nicholls, S., Chipperfield, M.P., Dalvi, M., Folberth, G.A.,
 1002 Dennison, F., Dhomse, S.S., Griffiths, P.T. and Hardacre, C., 2020a. Description and evaluation of the UKCA
 1003 stratosphere–troposphere chemistry scheme (StratTrop vn 1.0) implemented in UKESM1. *Geoscientific Model*
 1004 *Development*, 13(3), pp.1223-1266.

1005

1006 Archibald, A.T., Neu, J.L., Elshorbany, Y.F., Cooper, O.R., Young, P.J., Akiyoshi, H., Cox, R.A., Coyle, M.,
 1007 Derwent, R.G., Deushi, M. and Finco, A., 2020b. Tropospheric Ozone Assessment ReportA critical review of
 1008 changes in the tropospheric ozone burden and budget from 1850 to 2100. *Elementa: Science of the*
 1009 *Anthropocene*, 8(1).

1010



- 1011 Archer-Nicholls, S., Abraham, N.L., Shin, Y.M., Weber, J., Russo, M.R., Lowe, D., Utembe, S., O'Connor, F.M.,
 1012 Kerridge, B., Latter, B. and Siddans, R., 2020. The Common Representative Intermediates Mechanism version 2 in
 1013 the United Kingdom Chemistry and Aerosols Model. *Earth and Space Science Open Archive ESSOAr*.
 1014
- 1015 Butler, T.M., Taraborrelli, D., Brühl, C., Fischer, H., Harder, H., Martinez, M., Williams, J., Lawrence, M.G. and
 1016 Lelieveld, J., 2008. Improved simulation of isoprene oxidation chemistry with the ECHAM5/MESy chemistry-
 1017 climate model: lessons from the GABRIEL airborne field campaign.
 1018
- 1019 Bates, K.H. and Jacob, D.J., 2019. A new model mechanism for atmospheric oxidation of isoprene: global effects on
 1020 oxidants, nitrogen oxides, organic products, and secondary organic aerosol. *Atmospheric Chemistry & Physics*,
 1021 19(14).
 1022
- 1023 Chen, J., Liu, Y., Zhang, M. and Peng, Y., 2016. New understanding and quantification of the regime dependence of
 1024 aerosol-cloud interaction for studying aerosol indirect effects. *Geophysical Research Letters*, 43(4), pp.1780-1787.
 1025
- 1026 Crounse, J.D., Paulot, F., Kjaergaard, H.G. and Wennberg, P.O., 2011. Peroxy radical isomerization in the oxidation
 1027 of isoprene. *Physical Chemistry Chemical Physics*, 13(30), pp.13607-13613.
 1028
- 1029 Dupuy, E., Walker, K.A., Kar, J., Boone, C.D., McElroy, C.T., Bernath, P.F., Drummond, J.R., Skelton, R., McLeod,
 1030 S.D., Hughes, R.C. and Nowlan, C.R., 2009. Validation of ozone measurements from the Atmospheric Chemistry
 1031 Experiment (ACE). *Atmospheric Chemistry and Physics*, 9(2), pp.287-343.
 1032
- 1033 Edwards, P.M., Evans, M.J., Furneaux, K.L., Hopkins, J., Ingham, T., Jones, C., Lee, J.D., Lewis, A.C., Moller, S.J.,
 1034 Stone, D. and Whalley, L.K., 2013. OH reactivity in a South East Asian tropical rainforest during the Oxidant and
 1035 Particle Photochemical Processes (OP3) project. *Atmospheric Chemistry and Physics*, 13(18), pp.9497-9514.
 1036
- 1037 Eerdekens, G., Ganzeveld, L., Vilà-Guerau de Arellano, J., Klüpfel, T., Sinha, V., Yassaa, N., Williams, J., Harder,
 1038 H., Kubistin, D., Martinez, M., and Lelieveld, J.: Flux estimates of isoprene, methanol and acetone from airborne
 1039 PTR-MS measurements over the tropical rainforest during the GABRIEL 2005 campaign, *Atmos. Chem. Phys.*, 9,
 1040 4207–4227, <https://doi.org/10.5194/acp-9-4207-2009>, 2009.
 1041
- 1042 Emmons, L.K., Edwards, D.P., Deeter, M.N., Gille, J.C., Campos, T., Nédélec, P., Novelli, P. and Sachse, G., 2009.
 1043 Measurements of Pollution in the Troposphere (MOPITT) validation through 2006. *Atmospheric Chemistry and*
 1044 *Physics*, 9(5), pp.1795-1803.
 1045
- 1046 Fares, S., Mahmood, T., Liu, S., Loreto, F., and Centritto, M. (2011). Influence of growth temperature and measuring
 1047 temperature on isoprene emission, diffusive limitations of photosynthesis and respiration in hybrid poplars.
 1048 *Atmospheric Environment*, 45(1):155– 161



- 1049
- 1050 Gordon, H., Sengupta, K., Rap, A., Duplissy, J., Frege, C., Williamson, C., Heinritzi, M., Simon, M., Yan, C.,
 1051 Almeida, J., and Tröstl, J.: Reduced anthropogenic aerosol radiative forcing caused by biogenic new particle
 1052 formation, *P. Natl. Acad. Sci. USA*, 113, 12053–12058, <https://doi.org/10.1073/pnas.1602360113>, 2016
- 1053
- 1054 Griffiths, P.T., Murray, L.T., Zeng, G., Archibald, A.T., Emmons, L.K., Galbally, I., Hassler, B., Horowitz, L.W.,
 1055 Keeble, J., Liu, J. and Moeini, O., 2020. Tropospheric ozone in CMIP6 Simulations. *Atmospheric Chemistry and*
 1056 *Physics Discussions*, pp.1-50.
- 1057
- 1058 Guenther, A. B., Jiang, X., Heald, C. L., Sakulyanontvittaya, T., Duhl, T., Emmons, L. K., and Wang, X.: The Model
 1059 of Emissions of Gases and Aerosols from Nature version 2.1 (MEGAN2.1): an extended and updated framework for
 1060 modeling biogenic emissions, *Geoscientific Model Development*, 5, 1471–1492, [https://doi.org/10.5194/gmd-5-1471-](https://doi.org/10.5194/gmd-5-1471-2012)
 1061 <http://www.geosci-model-dev.net/5/1471/2012/>, 2012.
- 1062
- 1063 Heald, C. L., Wilkinson, M. J., Monson, R. K., Alo, C. A., Wang, G., and Guenther, A. (2009). Response of isoprene
 1064 emission to ambient co2 changes and implications for global budgets. *Global Change Biology*, 15(5):1127–1140.
- 1065
- 1066 Heinritzi, M., Dada, L., Simon, M., Stolzenburg, D., Wagner, A. C., Fischer, L., Ahonen, L. R., Amanatidis, S.,
 1067 Baalbaki, R., Baccarini, A., Bauer, P. S., Baumgartner, B., Bianchi, F., Brilke, S., Chen, D., Chiu, R., Dias, A.,
 1068 Dommen, J., Duplissy, J., Finkenzeller, H., Frege, C., Fuchs, C., Garmash, O.,
 1069 Hoesly, R. M., Smith, S. J., Feng, L., Klimont, Z., Janssens-Maenhout, G., Pitkanen, T., . . . Zhang, Q. (2018).
 1070 Historical (1750-2014) anthropogenic emissions of reactive gases and aerosols from the Community Emissions Data
 1071 System (CEDS). *Geoscientific Model Development*, 11 (1), 369–408. doi:10.5194/gmd-11-369-2018
- 1072
- 1073 Gordon, H., Granzin, M., El Haddad, I., He, X., Helm, J., Hofbauer, V., Hoyle, C. R., Kangasluoma, J., Keber, T.,
 1074 Kim, C., Kürten, A., Lamkaddam, H., Laurila, T. M., Lampilahti, J., Lee, C. P., Lehtipalo, K., Leiminger, M., Mai,
 1075 H., Makhmutov, V., Manninen, H. E., Marten, R., Mathot, S., Mauldin, R. L., Mentler, B., Molteni, U., Müller, T.,
 1076 Nie, W., Nieminen, T., Onnela, A., Partoll, E., Passananti, M., Petäjä, T., Pfeifer, J., Pospisilova, V., Quéléver, L. L.
 1077 J., Rissanen, M. P., Rose, C., Schobesberger, S., Scholz, W., Scholze, K., Sipilä, M., Steiner, G., Stozhkov, Y., Tauber,
 1078 C., Tham, Y. J., Vazquez-Pufleau, M., Virtanen, A., Vogel, A. L., Volkamer, R., Wagner, R., Wang, M., Weitz, L.,
 1079 Wimmer, D., Xiao, M., Yan, C., Ye, P., Zha, Q., Zhou, X., Amorim, A., Baltensperger, U., Hansel, A., Kulmala, M.,
 1080 Tomé, A., Winkler, P. M., Worsnop, D. R., Donahue, N. M., Kirkby, J., and Curtius, J.: Molecular understanding of
 1081 the suppression of new-particle formation by isoprene, *Atmos. Chem. Phys.*, 20, 11809–11821,
 1082 <https://doi.org/10.5194/acp-20-11809-2020>, 2020.
- 1083
- 1084 Hewitt, C.N., Lee, J.D., MacKenzie, A.R., Barkley, M.P., Carslaw, N., Carver, G.D., Chappell, N.A., Coe, H., Collier,
 1085 C., Commane, R. and Davies, F., 2010. Overview: oxidant and particle photochemical processes above a south-east



- Asian tropical rainforest (the OP3 project): introduction, rationale, location characteristics and tools. *Atmospheric Chemistry and Physics*, 10(1), pp.169-199.
- Jenkin, M.E., Watson, L.A., Utembe, S.R. and Shallcross, D.E., 2008. A Common Representative Intermediates (CRI) mechanism for VOC degradation. Part 1: Gas phase mechanism development. *Atmospheric Environment*, 42(31), pp.7185-7195.
- Jenkin, M. E., Young, J. C., and Rickard, A. R.: The MCM v3.3.1 degradation scheme for isoprene, *Atmos. Chem. Phys.*, 15, 11433–11459, <https://doi.org/10.5194/acp-15-11433-2015>, 2015.
- Jenkin, M. E., Khan, M. A. H., Shallcross, D. E., Bergström, R., Simpson, D., Murphy, K. L. C., and Rickard, A. R.: The CRI v2. 2 reduced degradation scheme for isoprene, *Atmos. Environ.*, 212, 172–182, <https://doi.org/10.1016/j.atmosenv.2019.05.055>, 2019.
- Jo, D.S., Hodzic, A., Emmons, L.K., Tilmes, S., Schwantes, R.H., Mills, M.J., Campuzano-Jost, P., Hu, W., Zaveri, R.A., Easter, R.C. and Singh, B., 2021. Future changes in isoprene-epoxydiol-derived secondary organic aerosol (IEPOX SOA) under the Shared Socioeconomic Pathways: the importance of physicochemical dependency. *Atmospheric Chemistry and Physics*, 21(5), pp.3395-3425.
- Karset, I.H.H., Berntsen, T.K., Storelvmo, T., Alterskjær, K., Grini, A., Olivié, D., Kirkevåg, A., Seland, Ø., Iversen, T. and Schulz, M., 2018. Strong impacts on aerosol indirect effects from historical oxidant changes. *Atmospheric Chemistry and Physics*, 18(10), pp.7669-7690.
- Kelly, J.M., Doherty, R.M., O'Connor, F.M. and Mann, G.W., 2018. The impact of biogenic, anthropogenic, and biomass burning volatile organic compound emissions on regional and seasonal variations in secondary organic aerosol. *Atmospheric Chemistry and Physics*, 18(10), pp.7393-7422.
- Khan, M.A.H., Schlich, B.L., Jenkin, M.E., Cooke, M.C., Derwent, R.G., Neu, J.L., Percival, C.J. and Shallcross, D.E., 2021. Changes to simulated global atmospheric composition resulting from recent revisions to isoprene oxidation chemistry. *Atmospheric Environment*, 244, p.117914
- Kiendler-Scharr, A., Wildt, J., Dal Maso, M., Hohaus, T., Kleist, E., Mentel, T.F., Tillmann, R., Uerlings, R., Schurr, U. and Wahner, A., 2009. New particle formation in forests inhibited by isoprene emissions. *Nature*, 461(7262), pp.381-384.
- Kirkby, J., Duplissy, J., Sengupta, K., Frege, C., Gordon, H., Williamson, C., Heinritzi, M., Simon, M., Yan, C., Almeida, J., and Tröstl, J.: Ion-induced nucleation of pure biogenic particles, *Nature*, 533, 521–526, <https://doi.org/10.1038/nature17953>, 2016.



- 1124
- 1125 Lelieveld, J., Butler, T.M., Crowley, J.N., Dillon, T.J., Fischer, H., Ganzeveld, L., Harder, H., Lawrence, M.G.,
 1126 Martinez, M., Taraborrelli, D. and Williams, J., 2008. Atmospheric oxidation capacity sustained by a tropical
 1127 forest. *Nature*, 452(7188), pp.737-740.
- 1128
- 1129 Liu, Z., Nguyen, V.S., Harvey, J., Müller, J.F. and Peeters, J., 2017. Theoretically derived mechanisms of HPALD
 1130 photolysis in isoprene oxidation. *Physical Chemistry Chemical Physics*, 19(13), pp.9096-9106.
- 1131
- 1132 Mann, G.W., Carslaw, K.S., Spracklen, D.V., Ridley, D.A., Manktelow, P.T., Chipperfield, M.P., Pickering, S.J. and
 1133 Johnson, C.E., 2010. Description and evaluation of GLOMAP-mode: A modal global aerosol microphysics model for
 1134 the UKCA composition-climate model. *Geoscientific Model Development*, 3(2), p.519.
- 1135
- 1136 McFiggans, G., Mentel, T.F., Wildt, J., Pullinen, I., Kang, S., Kleist, E., Schmitt, S., Springer, M., Tillmann, R., Wu,
 1137 C. and Zhao, D., 2019. Secondary organic aerosol reduced by mixture of atmospheric vapours. *Nature*, 565(7741),
 1138 pp.587-593.
- 1139
- 1140 Meenigen, Y.V., Schurgers, G., Rinnan, R. and Holst, T., 2017. Isoprenoid emission response to changing light
 1141 conditions of English oak, European beech and Norway spruce. *Biogeosciences*, 14(18), pp.4045-4060
- 1142
- 1143
- 1144 Metzger, A., Verheggen, B., Dommen, J., Duplissy, J., Prevot, A.S., Weingartner, E., Riipinen, I., Kulmala, M.,
 1145 Spracklen, D.V., Carslaw, K.S. and Baltensperger, U., 2010. Evidence for the role of organics in aerosol particle
 1146 formation under atmospheric conditions. *Proceedings of the National Academy of Sciences*, 107(15), pp.6646-6651.
- 1147
- 1148 Møller, K.H., Bates, K.H. and Kjaergaard, H.G., 2019. The importance of peroxy radical hydrogen-shift reactions in
 1149 atmospheric isoprene oxidation. *The Journal of Physical Chemistry A*, 123(4), pp.920-932.
- 1150
- 1151 Mulcahy, J.P., Johnson, C., Jones, C.G., Povey, A.C., Scott, C.E., Sellar, A., Turnock, S.T., Woodhouse, M.T.,
 1152 Abraham, N.L., Andrews, M.B. and Bellouin, N., 2020. Description and evaluation of aerosol in UKESM1 and
 1153 HadGEM3-GC3. 1 CMIP6 historical simulations. *Geoscientific Model Development Discussions*, pp.1-59.
- 1154
- 1155 Nguyen, T.B., Coggon, M.M., Bates, K.H., Zhang, X., Schwantes, R.H., Schilling, K.A., Loza, C.L., Flagan, R.C.,
 1156 Wennberg, P.O. and Seinfeld, J.H., 2014. Organic aerosol formation from the reactive uptake of isoprene epoxydiols
 1157 (IEPOX) onto non-acidified inorganic seeds. *Atmospheric Chemistry and Physics*, 14(7), pp.3497-3510.
- 1158
- 1159 Nguyen, T.B., Bates, K.H., Crounse, J.D., Schwantes, R.H., Zhang, X., Kjaergaard, H.G., Surratt, J.D., Lin, P., Laskin,
 1160 A., Seinfeld, J.H. and Wennberg, P.O., 2015. Mechanism of the hydroxyl radical oxidation of methacryloyl



- 1161 peroxyne (MPAN) and its pathway toward secondary organic aerosol formation in the atmosphere. *Physical*
 1162 *Chemistry Chemical Physics*, 17(27), pp.17914-17926.
- 1163
- 1164 O'Connor, F.M., Abraham, N.L., Dalvi, M., Folberth, G., Griffiths, P., Hardacre, C., Johnson, B.T., Kahana, R.,
 1165 Keeble, J., Kim, B. and Morgenstern, O., 2020. Assessment of pre-industrial to present-day anthropogenic climate
 1166 forcing in UKESM1. *Atmospheric Chemistry and Physics Discussions*, pp.1-49.
- 1167
- 1168 Olivier, J. G. J., Peters, J., Granier, C., Petron, G., Muller, J.-F., and Wallens, S.: Present and future surface emissions
 1169 of atmospheric compounds, POET Report #3, EU project EVK2-1999-00011, 2003.
- 1170
- 1171 Pacifico, F., Folberth, G.A., Jones, C.D., Harrison, S.P. and Collins, W.J., 2012. Sensitivity of biogenic isoprene
 1172 emissions to past, present, and future environmental conditions and implications for atmospheric chemistry. *Journal*
 1173 *of Geophysical Research: Atmospheres*, 117(D22).
- 1174
- 1175 Peeters, J., Nguyen, T.L. and Vereecken, L., 2009. HO x radical regeneration in the oxidation of isoprene. *Physical*
 1176 *Chemistry Chemical Physics*, 11(28), pp.5935-5939.
- 1177
- 1178 Peeters, J., Müller, J.F., Stavrakou, T. and Nguyen, V.S., 2014. Hydroxyl radical recycling in isoprene oxidation driven
 1179 by hydrogen bonding and hydrogen tunneling: The upgraded LIM1 mechanism. *The Journal of Physical Chemistry*
 1180 *A*, 118(38), pp.8625-8643.
- 1181
- 1182 Pétron, G., Granier, C., Khattatov, B., Lamarque, J. F., Yudin, V., Muller, J. F., & Gille, J. (2002). Inverse modeling
 1183 of carbon monoxide surface emissions using Climate Monitoring and Diagnostics Laboratory network observations.
 1184 *Journal of Geophysical Research Atmospheres*, 107 (24), 1 {23. doi:10.1029/2001JD001305
- 1185
- 1186 Prather, M.J., 2015. Photolysis rates in correlated overlapping cloud fields: Cloud-J 7.3 c, *Geosci. Model Dev.*, 8,
 1187 2587–2595.
- 1188
- 1189 Schwantes, R.H., Emmons, L.K., Orlando, J.J., Barth, M.C., Tyndall, G.S., Hall, S.R., Ullmann, K., St Clair, J.M.,
 1190 Blake, D.R., Wisthaler, A. and Bui, T.P.V., 2020. Comprehensive isoprene and terpene gas-phase chemistry improves
 1191 simulated surface ozone in the southeastern US. *Atmospheric Chemistry & Physics*, 20(6).
- 1192
- 1193 Scott, C.E., Rap, A., Spracklen, D.V., Forster, P.M., Carslaw, K.S., Mann, G.W., Pringle, K.J., Kivekas, N., Kulmala,
 1194 M., Lihavainen, H. and Tunved, P., 2014. The direct and indirect radiative effects of biogenic secondary organic
 1195 aerosol. *Atmospheric Chemistry and Physics*, 14(1), pp.447-470.
- 1196



- 1197 Sellar, A.A., Walton, J., Jones, C.G., Wood, R., Abraham, N.L., Andrejczuk, M., Andrews, M.B., Andrews, T.,
 1198 Archibald, A.T., de Mora, L. and Dyson, H., 2020. Implementation of UK Earth system models for CMIP6. *Journal*
 1199 *of Advances in Modeling Earth Systems*, 12(4), p.e2019MS001946.
- 1200
- 1201 Simon, M., Dada, L., Heinritzi, M., Scholz, W., Stolzenburg, D., Fischer, L., Wagner, A. C., Kürten, A., Rörup, B.,
 1202 He, X.-C., Almeida, J., Baalbaki, R., Baccarini, A., Bauer, P. S., Beck, L., Bergen, A., Bianchi, F., Bräkling, S., Brilke,
 1203 S., Caudillo, L., Chen, D., Chu, B., Dias, A., Draper, D. C., Duplissy, J., El-Haddad, I., Finkenzeller, H., Frege, C.,
 1204 Gonzalez-Carracedo, L., Gordon, H., Granzin, M., Hakala, J., Hofbauer, V., Hoyle, C. R., Kim, C., Kong, W.,
 1205 Lamkaddam, H., Lee, C. P., Lehtipalo, K., Leiminger, M., Mai, H., Manninen, H. E., Marie, G., Marten, R., Mentler,
 1206 B., Molteni, U., Nichman, L., Nie, W., Ojdanic, A., Onnela, A., Partoll, E., Petäjä, T., Pfeifer, J., Philippov, M.,
 1207 Quéléver, L. L. J., Ranjithkumar, A., Rissanen, M. P., Schallhart, S., Schobesberger, S., Schuchmann, S., Shen, J.,
 1208 Sipilä, M., Steiner, G., Stozhkov, Y., Tauber, C., Tham, Y. J., Tomé, A. R., Vazquez-Pufleau, M., Vogel, A. L.,
 1209 Wagner, R., Wang, M., Wang, D. S., Wang, Y., Weber, S. K., Wu, Y., Xiao, M., Yan, C., Ye, P., Ye, Q., Zauner-
 1210 Wieczorek, M., Zhou, X., Baltensperger, U., Dommen, J., Flagan, R. C., Hansel, A., Kulmala, M., Volkamer, R.,
 1211 Winkler, P. M., Worsnop, D. R., Donahue, N. M., Kirkby, J., and Curtius, J.: Molecular understanding of new particle
 1212 formation from α -pinene between -50 and C25 C, *Atmos. Chem. Phys.*, 20, 9183–9207, [https://doi.org/10.5194/acp-](https://doi.org/10.5194/acp-20-9183-2020)
 1213 20-9183-2020, 2020.
- 1214
- 1215 Sindelarova, K., Granier, C., Bouarar, I., Guenther, A., Tilmes, S., Stavrakou, T., Müller, J.-F., Kuhn, U., Stefani, P.,
 1216 and Knorr, W.: Global data set of biogenic VOC emissions calculated by the MEGAN model over the last 30 years,
 1217 *Atmos. Chem. Phys.*, 14, 9317–9341, <https://doi.org/10.5194/acp-14-9317-2014>, 2014.
- 1218
- 1219 Sporre, M.K., Blichner, S.M., Karset, I.H., Makkonen, R. and Berntsen, T.K., 2019. BVOC–aerosol–climate
 1220 feedbacks investigated using NorESM. *Atmospheric Chemistry and Physics*, 19(7), pp.4763–4782.
- 1221
- 1222 Sporre, M.K., Blichner, S.M., Schrödner, R., Karset, I.H., Berntsen, T.K., Noije, T.V., Bergman, T., O'Donnell, D.
 1223 and Makkonen, R., 2020. Large difference in aerosol radiative effects from BVOC-SOA treatment in three Earth
 1224 system models. *Atmospheric Chemistry and Physics*, 20(14), pp.8953–8973.
- 1225
- 1226 Squire, O.J., Archibald, A.T., Griffiths, P.T., Jenkin, M.E., Smith, D. and Pyle, J.A., 2015. Influence of isoprene
 1227 chemical mechanism on modelled changes in tropospheric ozone due to climate and land use over the 21st century.
 1228 *Atmospheric Chemistry and Physics*, 15(9), p.5123.
- 1229
- 1230 Telford, P.J., Abraham, N.L., Archibald, A.T., Braesicke, P., Dalvi, M., Morgenstern, O., O'Connor, F.M., Richards,
 1231 N.A.D. and Pyle, J.A., 2012. Implementation of the Fast-JX Photolysis scheme into the UKCA component of the
 1232 MetUM chemistry climate model. *Geosci. Model Dev. Discuss.*, 5, pp.3217–3260.
- 1233



- 1234 Teng, A.P., Crounse, J.D. and Wennberg, P.O., 2017. Isoprene peroxy radical dynamics. *Journal of the American*
 1235 *Chemical Society*, 139(15), pp.5367-5377.
- 1236
- 1237 Thornhill, G., Collins, W., Olivie, D., Skeie, R. B., Archibald, A., Bauer, S., Checa-Garcia, R., Fiedler, S., Folberth,
 1238 G., Gjermundsen, A., Horowitz, L., Lamarque, J.-F., Michou, M., Mulcahy, J., Nabat, P., Naik, V., O'Connor, F. M.,
 1239 Paulot, F., Schulz, M., Scott, C. E., Séférian, R., Smith, C., Takemura, T., Tilmes, S., Tsigaridis, K., and Weber, J.:
 1240 Climate-driven chemistry and aerosol feedbacks in CMIP6 Earth system models, *Atmos. Chem. Phys.*, 21, 1105–
 1241 1126, <https://doi.org/10.5194/acp-21-1105-2021>, 2021.
- 1242
- 1243 Tilmes, S., Lamarque, J.-F., Emmons, L. K., Conley, A., Schultz, M. G., Saunio, M., Thouret, V., Thompson, A. M.,
 1244 Oltmans, S. J., Johnson, B., and Tarasick, D.: Technical Note: Ozone sonde climatology between 1995 and 2011:
 1245 description, evaluation and applications, *Atmos. Chem. Phys.*, 12, 7475–7497, [https://doi.org/10.5194/acp-12-7475-](https://doi.org/10.5194/acp-12-7475-2012)
 1246 2012, 2012.
- 1247
- 1248 Toon, O.B., Maring, H., Dibb, J., Ferrare, R., Jacob, D.J., Jensen, E.J., Luo, Z.J., Mace, G.G., Pan, L.L., Pfister, L.
 1249 and Rosenlof, K.H., 2016. Planning, implementation, and scientific goals of the Studies of Emissions and Atmospheric
 1250 Composition, Clouds and Climate Coupling by Regional Surveys (SEAC4RS) field mission. *Journal of Geophysical*
 1251 *Research: Atmospheres*, 121(9), pp.4967-5009.
- 1252
- 1253 Twomey, S.J.A.E., 1974. Pollution and the planetary albedo. *Atmospheric Environment* (1967), 8(12), pp.1251-1256.
- 1254
- 1255 Utembe, S.R., Cooke, M.C., Archibald, A.T., Jenkin, M.E., Derwent, R.G. and Shallcross, D.E., 2010. Using a reduced
 1256 Common Representative Intermediates (CRIv2-R5) mechanism to simulate tropospheric ozone in a 3-D Lagrangian
 1257 chemistry transport model. *Atmospheric Environment*, 44(13), pp.1609-1622.
- 1258
- 1259 Watson, L.A., Shallcross, D.E., Utembe, S.R. and Jenkin, M.E., 2008. A Common Representative Intermediates (CRI)
 1260 mechanism for VOC degradation. Part 2: Gas phase mechanism reduction. *Atmospheric Environment*, 42(31),
 1261 pp.7196-7204.
- 1262
- 1263
- 1264 Weber, J., Shin, Y.M., Staunton Sykes, J., Archer-Nicholls, S., Abraham, N.L. and Archibald, A.T., 2020a. Minimal
 1265 Climate Impacts From Short-Lived Climate Forcers Following Emission Reductions Related to the COVID-19
 1266 Pandemic. *Geophysical research letters*, 47(20), p.e2020GL090326.
- 1267
- 1268 Weber, J., Archer-Nicholls, S., Griffiths, P., Berndt, T., Jenkin, M., Gordon, H., Knote, C. and Archibald, A.T., 2020b.
 1269 CRI-HOM: A novel chemical mechanism for simulating highly oxygenated organic molecules (HOMs) in global
 1270 chemistry–aerosol–climate models. *Atmospheric Chemistry and Physics*, 20(18), pp.10889-10910.
- 1271



- 1272 Wells, K.C., Millet, D.B., Payne, V.H., Deventer, M.J., Bates, K.H., de Gouw, J.A., Graus, M., Warneke, C.,
 1273 Wisthaler, A. and Fuentes, J.D., 2020. Satellite isoprene retrievals constrain emissions and atmospheric
 1274 oxidation. *Nature*, 585(7824), pp.225-233.
- 1275
- 1276 Wennberg, P.O., Bates, K.H., Crounse, J.D., Dodson, L.G., McVay, R.C., Mertens, L.A., Nguyen, T.B., Praske, E.,
 1277 Schwantes, R.H., Smarte, M.D. and St Clair, J.M., 2018. Gas-phase reactions of isoprene and its major oxidation
 1278 products. *Chemical reviews*, 118(7), pp.3337-3390.
- 1279
- 1280 Whalley, L.K., Edwards, P.M., Furneaux, K.L., Goddard, A., Ingham, T., Evans, M.J., Stone, D., Hopkins, J.R., Jones,
 1281 C.E., Karunaharan, A. and Lee, J.D., 2011. Quantifying the magnitude of a missing hydroxyl radical source in a
 1282 tropical rainforest. *Atmospheric Chemistry and Physics*, 11(14), pp.7223-7233.
- 1283
- 1284
- 1285 Zhu, J., Penner, J.E., Yu, F., Sillman, S., Andreae, M.O. and Coe, H., 2019. Decrease in radiative forcing by organic
 1286 aerosol nucleation, climate, and land use change. *Nature communications*, 10(1), pp.1-7.
- 1287
- 1288
- 1289
- 1290
- 1291

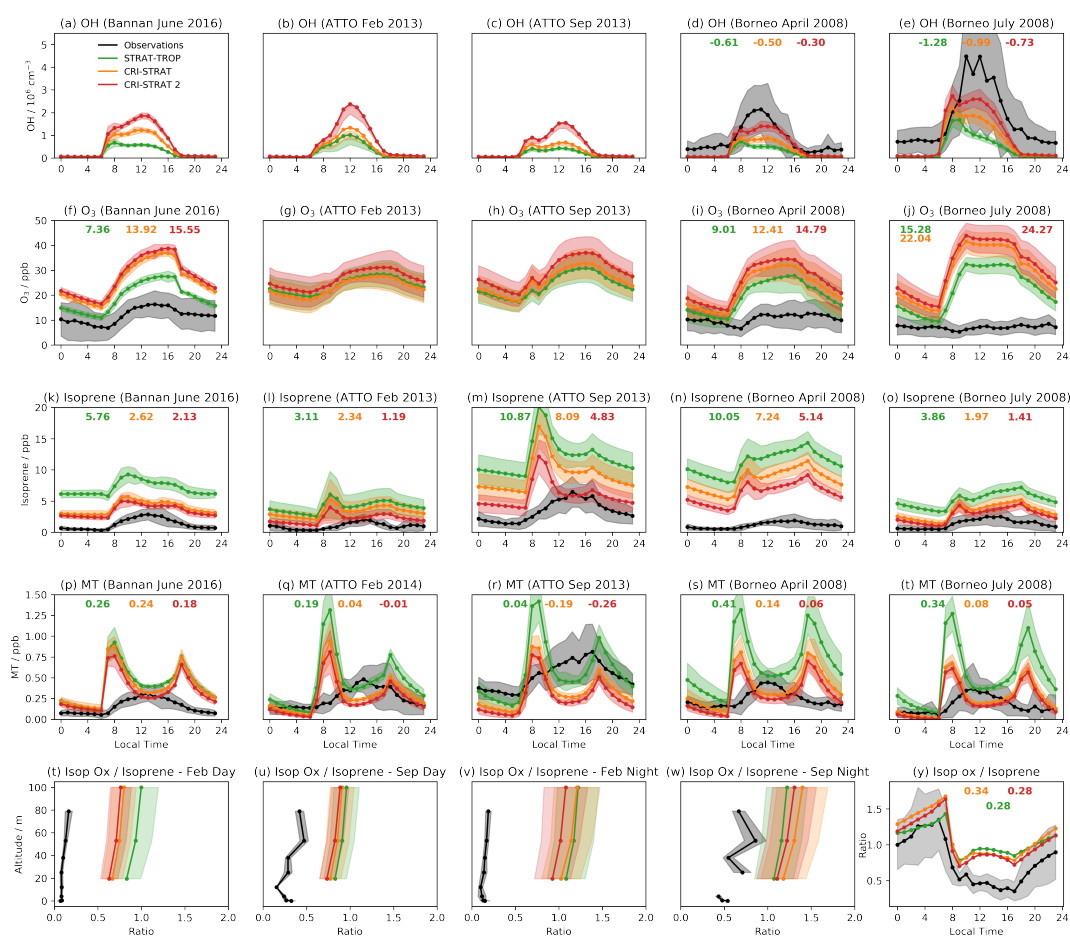


Figure 1. Mean diel cycles of observed and modelled OH (top row), O₃ (2nd row), Isoprene (3rd row) and MT (MT=α-pinene + β-pinene for the CRI mechanisms) (4th row) at the three surface/near surface sites considered. The bottom row shows the vertical profile of the ratio of isoprene oxidation products to isoprene for daytime (0900-1500 LT) and nighttime (2100-0300 LT) periods and the diel profile of the ratio at 53 m (all from ATTO tower). Shading indicates ±1 standard deviation from the mean and the numbers in bold show the mean diel model bias (model - observations) for species/locations where observations were recorded.

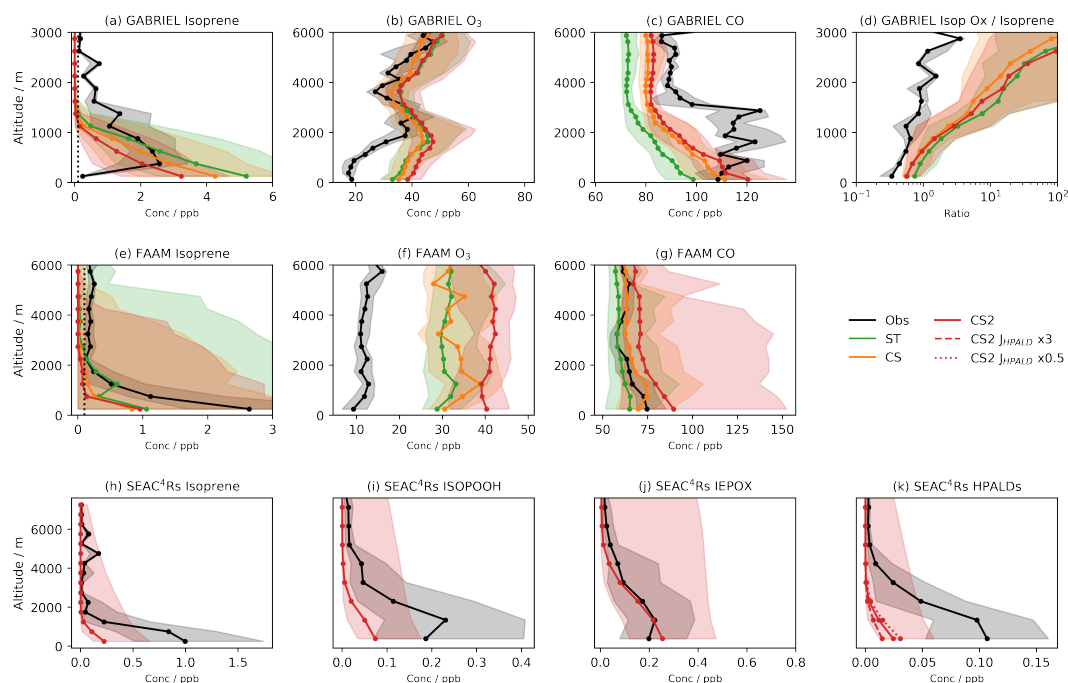


Figure 2. Median observed and model concentrations for the GABRIEL campaign in the Amazon for (a) Isoprene, (b) O₃, (c) CO and (d) the ratio of isoprene oxidation products to isoprene. Median observed and model concentrations for the FAAM campaign over Borneo for (e) isoprene, (f) O₃ and (g) CO. Median observed and model concentrations for the SEAC⁴RS campaign over the South East USA for (h) isoprene, (i) isoprene hydroperoxide (ISOPOOH), (j) the isoprene epoxy diol (IEPOX) and (k) hydroperoxy aldehydes (HPALDs). SEAC⁴RS observational data is also filtered to exclude urban plumes (NO₂>4 ppb), fire plumes (acetonitrile>0.2 ppb) and stratospheric air (O₃/CO > 1.25) as done in Schwantes et al (2020). Shading shows IQR, black dotted lines (a, e) show estimated limits of detection for isoprene and JHPALDx3 and JHPALDx0.5 lines in (k) show results of the scaling the HPALD photolysis frequency by 3 and 0.5, respectively. Note the logarithmic horizontal scale for (d).

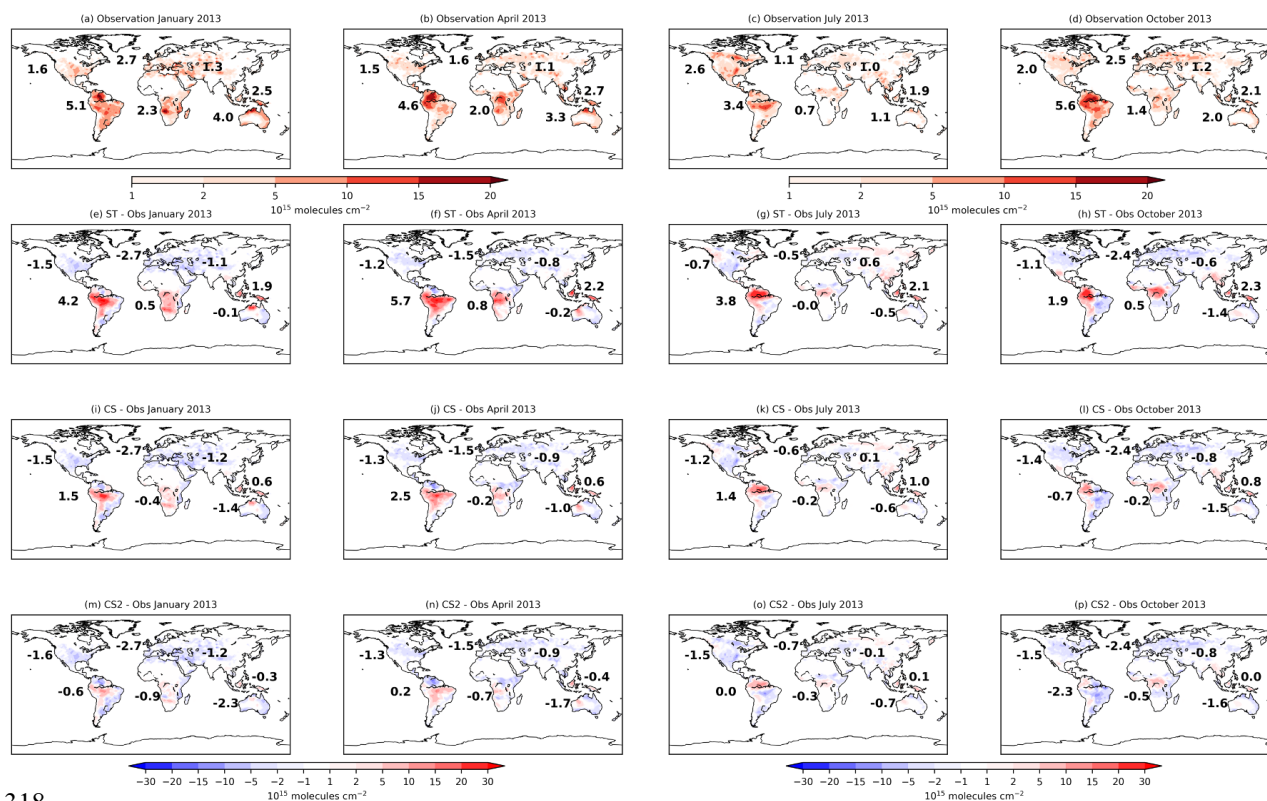


Figure 3. Monthly mean isoprene column values from the Global Isoprene Column observational dataset (Wells et al., 2020) for (a) January, (b) April, (c) July and (d) October 2013. Model bias (model-observation) using (d-h) ST (i-l) CS, and (m-p) CS2. Numbers in (a-d) show area-weighted mean model column values and in (e-p) model bias for individual terrestrial regions (number in North Atlantic refers to Europe and South Atlantic to Africa).

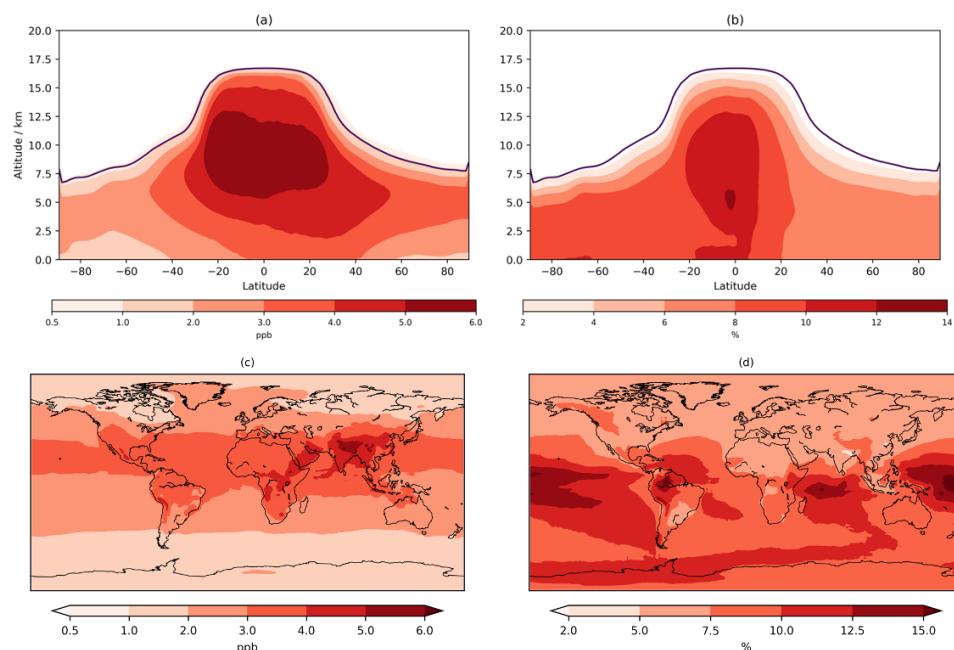


Figure 4. Annual mean tropospheric zonal (a, b) and lowest 500 m (c, d) change in O_3 mixing ratio (CS2 - CS). Purple line in zonal mean shows average height of tropopause.

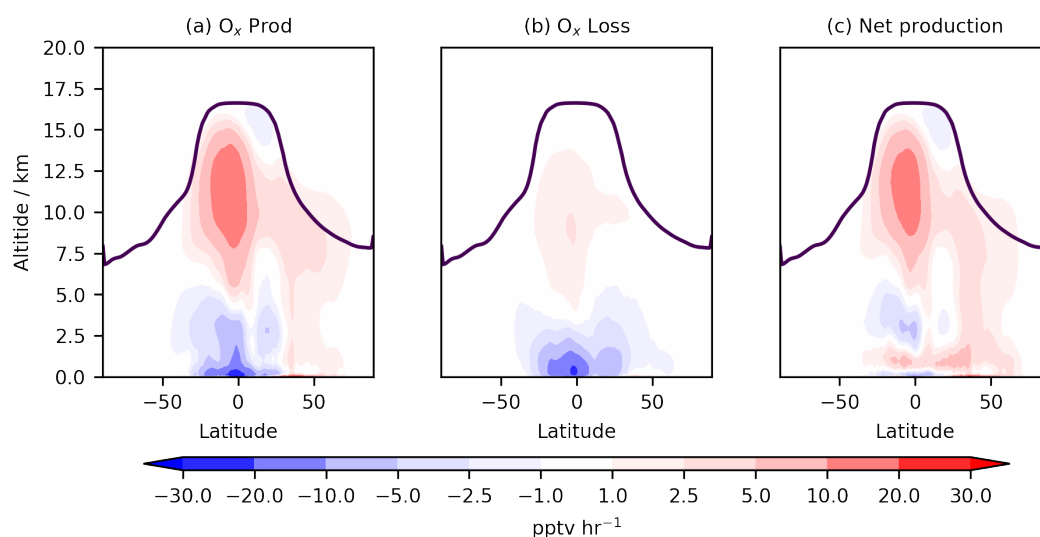


Figure 5. Annual zonal mean change in (a) total O_x production flux, (b) total O_x chemical loss flux and (c) net O_x chemical production flux. Purple line indicates mean tropopause height.

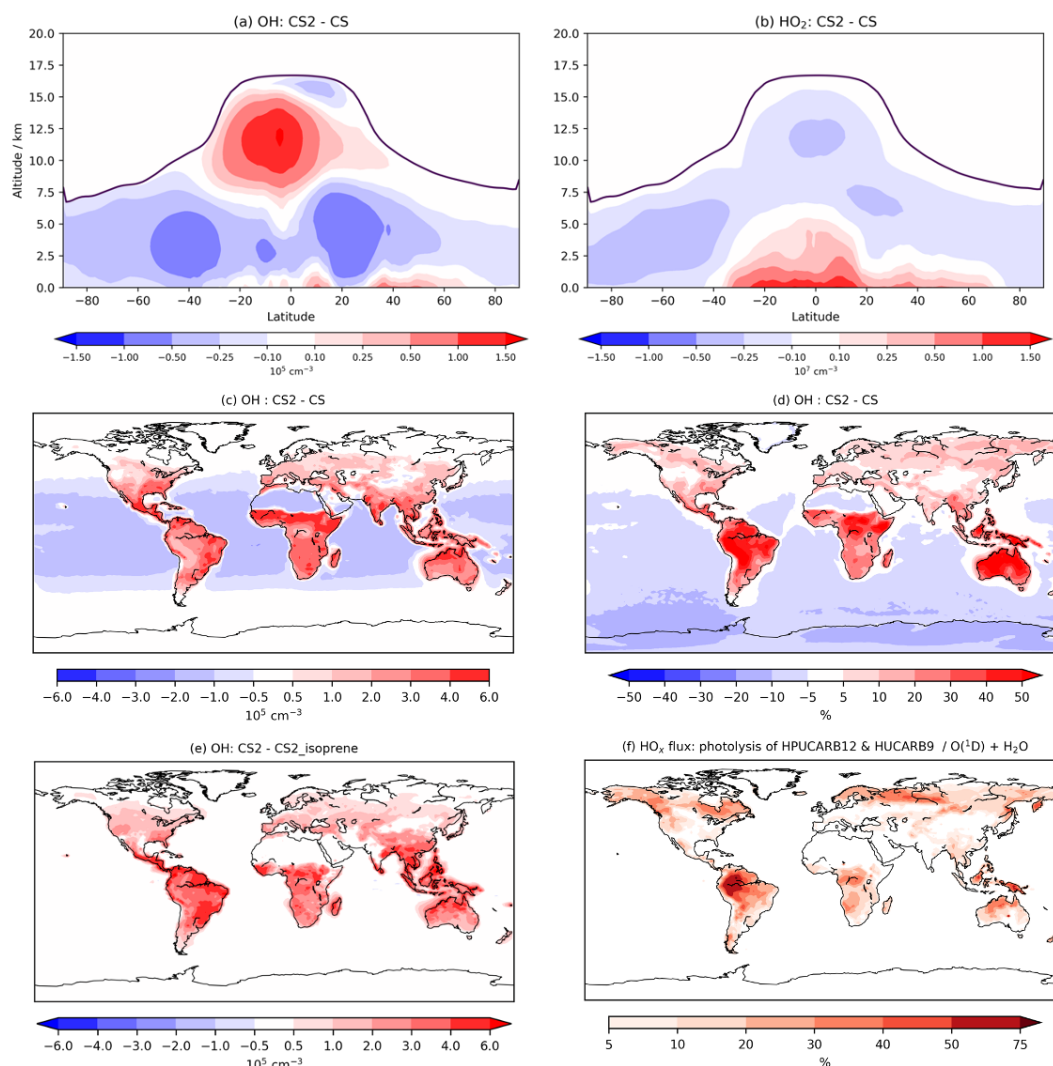


Figure 6. Annual zonal mean changes in (a) OH and (b) HO₂ between CS₂ and CS, (c) absolute and (d) percentage in change in OH in lowest ~500 m of atmosphere, (e) the change in OH in lowest 500 m between the CS₂ and CS₂_isoprene sensitivity test and (f) HO_x production flux from HPUCARB12 and HUCARB9 photolysis as a percentage of HO_x from O(¹D) + H₂O (right, bottom). Purple lines indicate average height of tropopause.

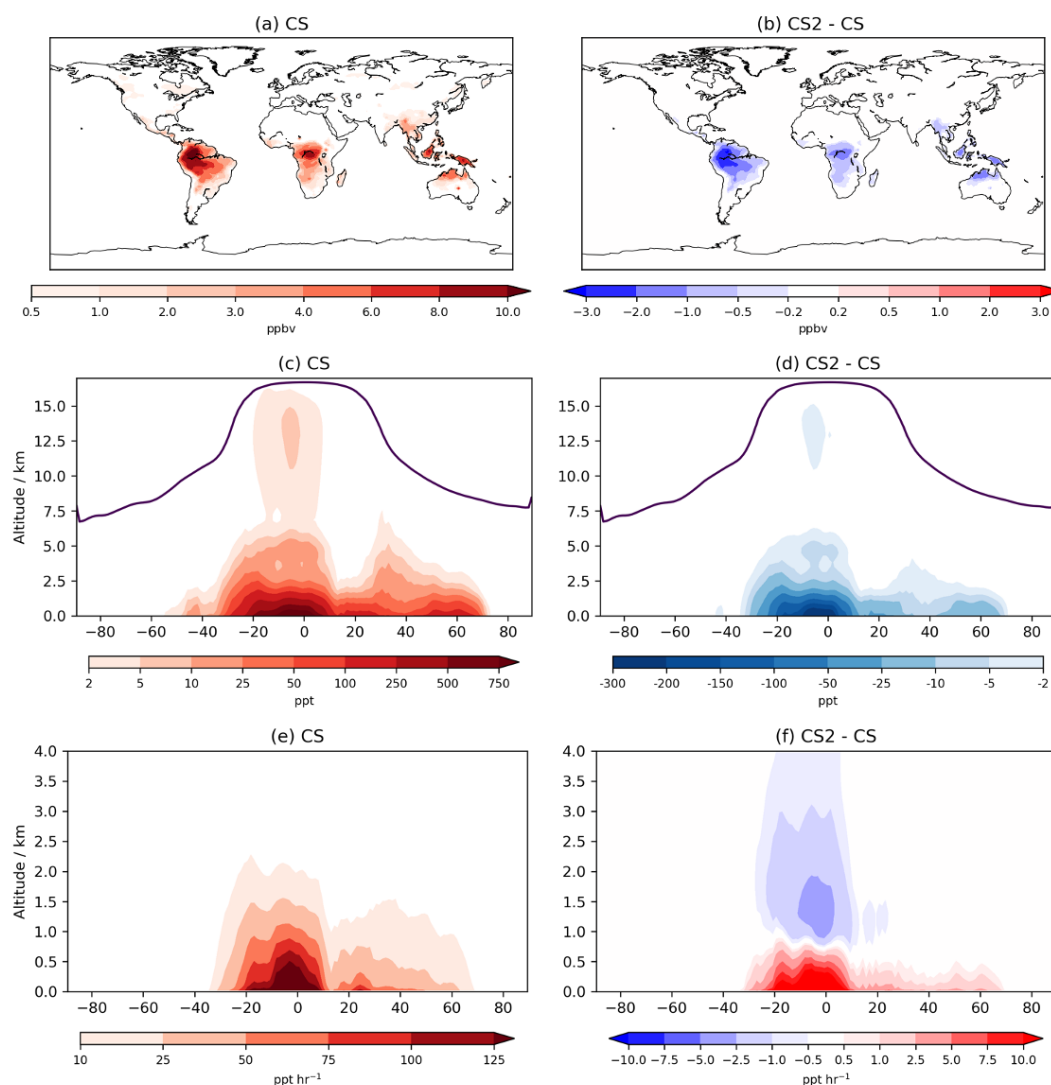


Figure 7. Annual mixing ratio of isoprene averaged over the lowest ~ 100 m (a) in CS and (b) the difference between CS2 and CS. Annual zonal mean mixing ratios in (c) CS and (d) difference between CS2 and CS (note the log scales). Annual average total oxidation flux of isoprene (e) in CS and (f) the difference between CS2 and CS.

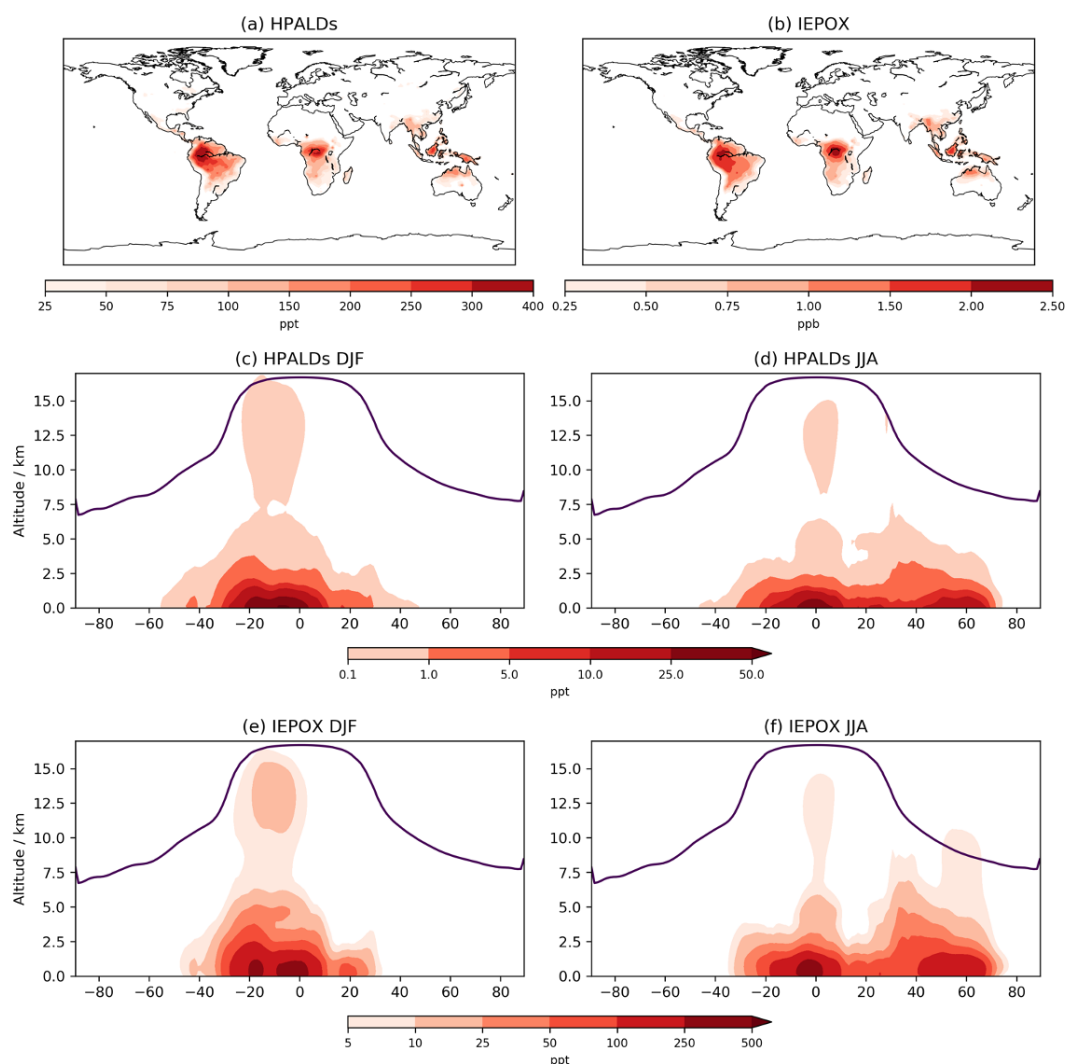


Figure 8. Annual mean mixing ratios for (a) HPALDs and (b) IEPOX (upper panels) over lowest ~100 m. DJF and JJA zonal mean mixing ratios for HPALDs (c, d) and IEPOX (e,f), note differing scales for HPALD and IEPOX plots and log scales for (c-f).

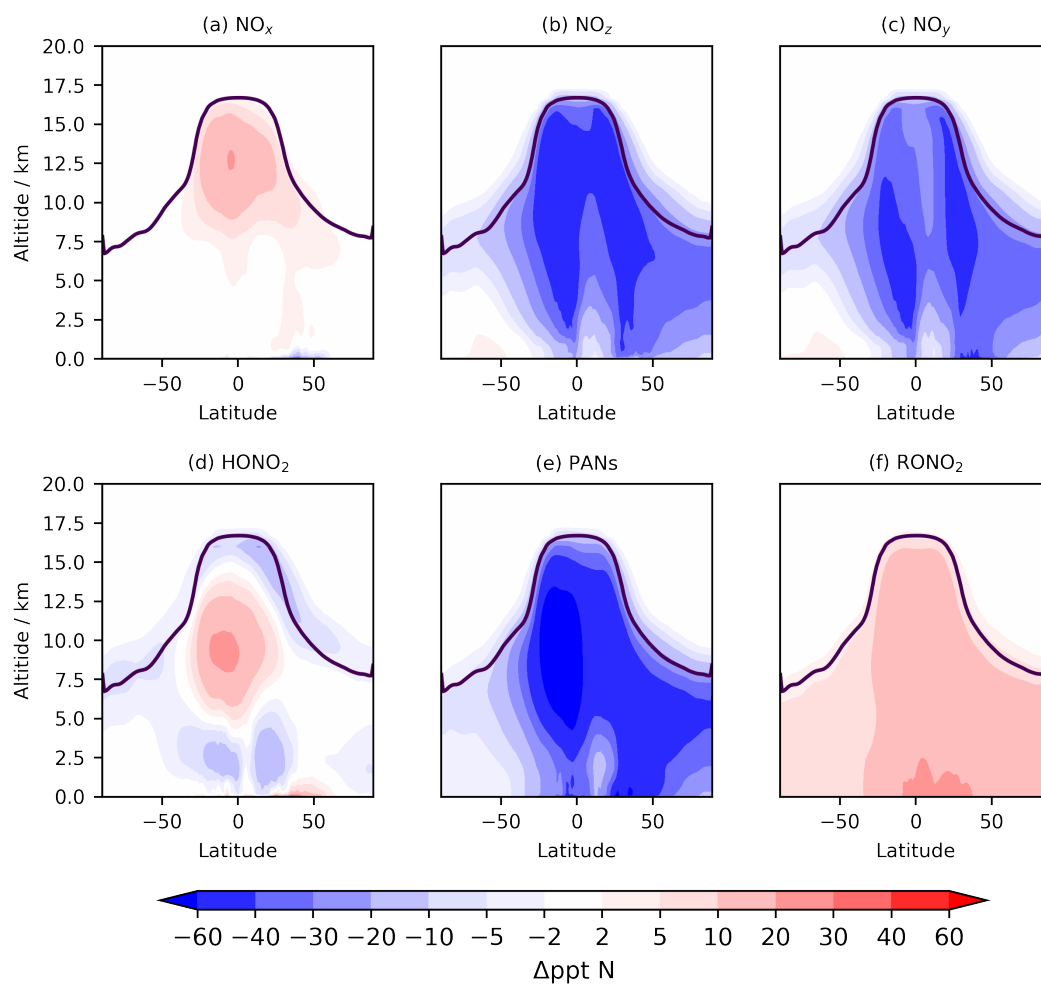


Figure 9. Tropospheric annual zonal mean change in (a) NO_x, (b) NO_z, (c) NO_y, (d) HONO₂, (e) PANs and (f) RONO₂ between CS2 and CS. Purple line shows average tropopause height.

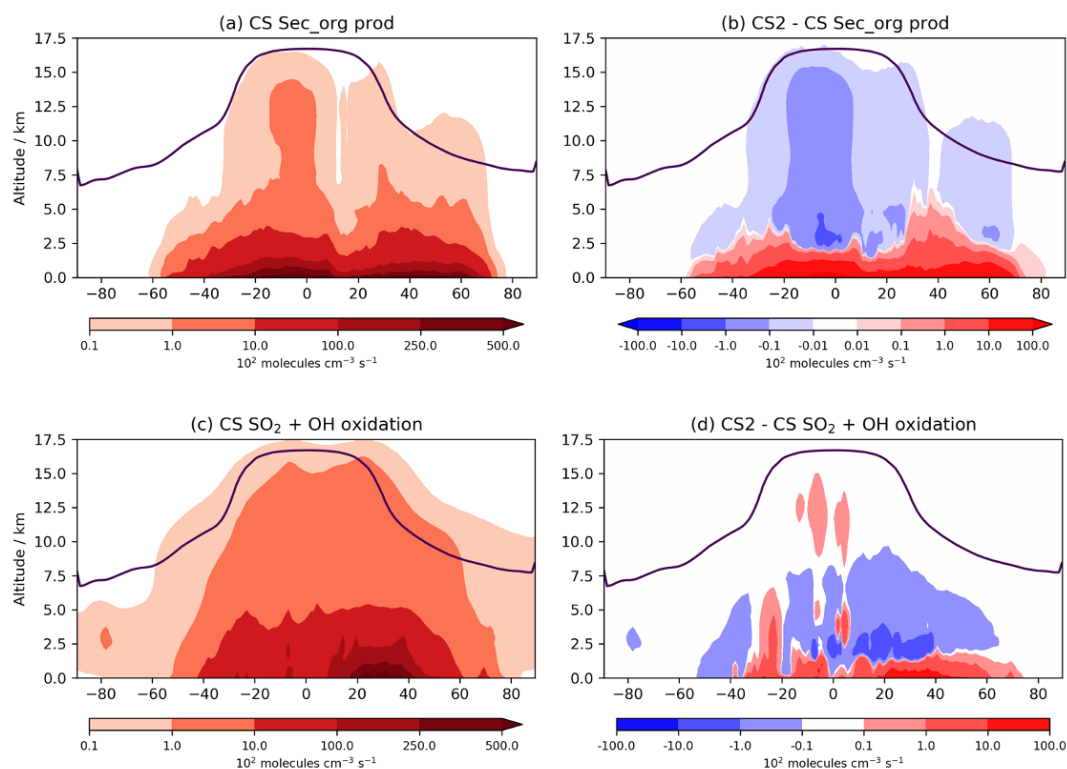


Figure 10. Tropospheric annual zonal mean production flux of Sec_Org in (a) CS and (b) difference between CS2 and CS. Annual zonal mean flux of SO₂ + OH in (c) CS and (d) difference between CS2 and CS.

Table 1. Comparison of the CRI-STRAT and CRI-STRAT 2 chemical mechanisms

	CRI-STRAT (CS)	CRI-STRAT 2 (CS2)
Tropospheric Chemistry Scheme	CRI v2.1 (Jenkin et al., 2008, Watson et al., 2008, Utembe et al., 2010)	CRI v2.2 (Jenkin et al., 2019)
Stratospheric Chemistry Scheme	Stratospheric chemistry (Morgenstern et al., 2009; Archibald et al., 2020)	Stratospheric chemistry (Morgenstern et al., 2009; Archibald et al., 2020)
No. of Species	219	228



No. of Bimolecular Reactions	536	582
No. of Termolecular Reactions	36	44
No. of Photolysis Reactions	128	140

Table 2. Species added and removed from the CS mechanism in the development of the CRI-Strat 2 mechanism.

Added Species	Species Functionality	MCM v3.3.1 equivalent
HPUCARB12	Hydroperoxy aldehyde (HPALD)	C5HPALD1, C5HPALD2
HUCARB9	Unsaturated hydroxy carbonyl	HMVK, HMAc
IEPOX	Isoprene epoxy diol	IEPOXA, IEPOXB, IEPOXC
HMML	Hydroxymethyl-methyl- α -lactone	HMML
DHPCARB9	Dihydroperoxy carbonyl	DHPMEK, DHPMPAL
DHPR12OOH	Trihydroperoxy carbonyl	C536OOH
DHCARB9	Dihydroxy carbonyl	HO12CO3C4
RU12NO3	Hydroxy carbonyl nitrate	C57NO3, C58NO3, C58ANO3
RU10NO3	Hydroxy carbonyl nitrate	MVKNO3, MACRNO3
DHPR12O2	Dihydroperoxy carbonyl peroxy radical	C536O2, C537O2
MACO3	Unsaturated acyl peroxy radical	MACO3
RU10AO2	Hydroxy carbonyl peroxy radical	MACRO2



Removed Species		MCM v3.2 equivalent
RU12PAN	PAN-type species with at least one hydroxy group	C5PAN19
TNCARB11	Alkyl carbonyl	N/A
TNCARB12	Alkyl carbonyl	N/A

Table 3 - Shorter runs performed for mechanism-observation comparisons. Identical biogenic (2001-2010 MEGAN-MACC climatology, iBVOC for isoprene and MT) and ocean (1990 timeslice) for each run unless otherwise stated.

Run Name	Mechanisms Tested	Period(s)	Observational Reference
ATTO	ST, CS, CS2	Feb 2013, Sept 2013, Feb 2014	Yanez-Serrano et al (2015)
ZF2 Brazil	ST, CS, CS2	June 2016	See SI Section S4
Borneo	ST, CS, CS2	April-May, June-July 2008	Hewitt et al (2010), Whalley et al (2011), Edwards et al (2013)
GABRIEL	ST, CS, CS2	October 2005	Butler et al (2008)
FAAM	ST, CS, CS2	July 2008	Hewitt et al (2010)
Isoprene Column	ST, CS, CS2	Jan, April, Jul & Oct 2013	Wells et al (2020)
SEAC ⁴ RS	CS2	August-September 2013	Toon et al (2016)

Table 4 - Longer runs performed for CRI mechanism comparison. Identical emissions for each run (anthropogenic and biomass timeslice 2014, biogenic 2001-2010 MEGAN-MACC climatology, oceanic 1990 timeslice)



Name	Base Mechanism	Total Length and Period	Alterations from base mechanism
CS	CRI-STRAT	5 years (1 year spin up)	None
CS2	CRI-STRAT 2	5 years (1 year spin up)	None
CS2_O1D	CS2	2 years (1 year spin up)	Rate constants for O(¹ D) with H ₂ O, O ₂ and N ₂ set to values in CS
CS2_inorgN	CS2	2 years (1 year spin up)	Rate constants for HONO ₂ , HO ₂ NO ₂ , N ₂ O ₅ , PAN formation, HO ₂ + NO and MeONO ₂ + OH set to values in CS
CS2_isoprene	CS2	2 years (1 year spin up)	Isoprene chemistry set to that in CS
CS2_RO2_N	CS2	2 years (1 year spin up)	Rate constants for RO ₂ + NO and RO ₂ + NO ₃ reactions reverted to CS values
CS2_photo (see SI Section 6)	CS2	2 years (1 year spin up)	Photolysis of CARB3, HCHO and EtCHO reverted to that from CS

Table 5. Location, reference, time period and species measured in observational data sets and corresponding modelling approach. For the Z2F Brazil, ATTO, Borneo, GABRIEL, FAAM and SE4C⁴RS datasets, model data was filtered to select only the same days as observational data.

Dataset	Reference	Dates of	Measurement	Species	Corresponding
---------	-----------	----------	-------------	---------	---------------



(Location / Coordinates)		Measurement	Details	Considered	model run (Table 3 unless stated)
ZF2 Brazil Field Campaign, Amazon (-2.60°, -60.21°, 60 km NNW of Manaus)	See SI Section S4	22 June 2016 - 5 July 2016	1-minute interval measurements 30 m above ground (above tree canopy)	O ₃ , CO, SO ₂ , NO ₂ , isoprene, monoterpenes, benzene	ZF2 Brazil
Instant ATTO Tower, Amazon (-2.14° , -59.00°, 150 km NE of Manaus)	Yannez-Serrano et al (2015)	February 2013, September 2013 and February 2014	16-minute interval measurements at multiple heights above ground (0.05 m, 0.5 m, 4 m, 12 m, 25 m, 38m, 53m and 79 m)	Isoprene, monoterpenes, methyl vinyl ketone (MVK), methacrolein (MACR), isoprene hydroperoxide (ISOPOOH), acetone (All PTRMS)	ATTO
GAW Station, Borneo (5.0°, 117.5°)	Hewitt et al (2010), Whalley et al (2011), Edwards et al (2013)	April-July 2008	10-minute intervals	OH, HO ₂ (both FAGE), O ₃ (Thermo Electron Instrument), isoprene, monoterpene (both PTRMS), HCHO (aerolaser Hantzsch), CO (Aerolaser AL5002), MeCHO, acetone MACR,	Borneo



				MVK (both GC-FID), PAN (GC-MS), NO ₂ (Thermo Environmental Instruments 42C)	
GABRIEL Aircraft Campaign (Suriname, Guyana and French Guiana)	Butler et al (2008)	October 2005	Daytime aircraft measurements sampling ~0.3-8 km at 30 second intervals	O ₃ , NO (both ECOEX), HCHO, CO (both MPIC TRISTAR), acetone, isoprene, MACR, MVK (all PTRMS)	GABRIEL
FAAM Aircraft Campaign, Borneo	Hewitt et al (2010)	July 2008	Daytime aircraft measurements sampling ~0.3-7 km at 5 min intervals	O ₃ (TECO 49), isoprene (PTRMS), CO (AERO AL5002)	FAAM
SE4C ⁴ RS Flight Campaign (Southeast United States)	Toon et al (2016)	August - September 2013	Daytime aircraft measurements sampling up to 12 km at 1 min intervals	O ₃ (ERSL), CO (DACOM), Isoprene (WAS), ISOPOOH, HPALDs, IEPOX, isoprene nitrate (all CIT)	SEAC ⁴ RS
Global Isoprene Columns	Wells et al (2020)	Jan, April, Jul & Oct 2013	Global monthly mean isoprene column values	Isoprene	Isoprene Column

1391
 1392
 1393



Table 6 - Annual mean O_x diagnostics for CRI-STRAT, CRI-STRAT 2 and difference between mechanisms (percentage changes in parentheses). UKESM1 CMIP6 1995-2004 using ST: chemical production = 5315 Tg year⁻¹, chemical loss = 4476 Tg year⁻¹, dry deposition = 867 Tg year⁻¹ (Griffiths et al., 2021)

	CS	CS2	CS2 - CS
O ₃ Burden (Tg)	328	354	26 (7.9%)
O _x Lifetime (days)	17.4	18.8	1.4 (8.0%)
OPE	33.74	33.78	0.05 (0.1%)
Chemical Production (Tg year⁻¹)	6572	6582	10 (0.1%)
HO ₂ + NO	4099	4322	132 (3.2%)
MeOO + NO	1573	1583	10 (0.6%)
NO + RO ₂	849	717	-131 (-15.4%)
Other	51	49	-1 (-2.8%)
Chemical Loss (Tg year⁻¹)	5834	5757	-77 (1.3%)
O(¹ D) + H ₂ O	3157	2928	-229 (-7.2%)
HO ₂ + O ₃	1666	1819	152 (9.1%)
OH + O ₃	740	796	57 (7.6%)
O ₃ + Alkene	166	101	-65 (-39.2%)
Other	105	113	8 (10.1%)
Deposition (Tg year⁻¹)	1133	1207	76 (6.5%)
O ₃ Dry Dep	942	1018	77 (8.0%)
NO _y dep	191	189	-3 (1.3%)
Inferred STT (Tg year ⁻¹)	395	384	-13 (-3.3%)



Table 7 – Tropospheric average HO_x parameters for CS and CS2.

	CS	CS2	CS2 – CS
[OH] / 10 ⁶ cm ⁻³	1.355	1.334	-0.021 (1.5%)
[HO ₂] / 10 ⁸ cm ⁻³	0.990	0.988	-0.002 (0.2%)
[OH] / [HO ₂] (%)	1.369	1.349	-0.02 (1.5%)
CH ₄ lifetime w.r.t. OH / years	7.43	7.60	-0.17 (2.3%)

Table 8 - Burdens of NO_y and its constituent species, NO_x emissions, NO_y deposition and inferred Stratosphere-to-Troposphere (STT) transport of NO_y. Values in parentheses for burdens show the fraction of total NO_y burden represented by each constituent and, for deposition diagnostics, the fraction of total NO_y deposition represented by each pathway.

	CS	CS2	CS2 – CS
NO_y burden / TgN	1.088	1.036	-0.052
NO _x burden / TgN	0.118 (10.9%)	0.123 (11.9%)	0.005
NO _z burden / TgN	0.972 (89.2%)	0.914 (88.1%)	-0.058
HONO ₂ burden / TgN	0.523 (48.0%)	0.521 (50.3%)	-0.002
Other inorganic NO _z burden / TgN	0.020 (1.8%)	0.014 (1.4%)	-0.006
PANs burden / TgN	0.367 (33.7%)	0.292 (28.2%)	-0.075
RONO ₂ burden / TgN	0.044 (4.0%)	0.070 (6.7%)	0.026
MeO ₂ NO ₂ burden / TgN	0.008 (0.8%)	0.008 (0.7%)	-0.0007



Nitrophenols burden / TgN	0.009 (0.9%)	0.009 (0.9%)	-0.0005
NO_x Emissions / TgN year⁻¹	55.65	55.65	0
Total NO_y Deposition / TgN year⁻¹	62.12	62.35	0.23
Inferred STT / TgN year⁻¹	6.47	6.70	0.23
NO _x Deposition / TgN year ⁻¹	6.32 (10.2 %)	6.30 (10.1 %)	-0.02
HONO ₂ Wet Deposition / TgN year ⁻¹	29.01 (46.6%)	29.26 (46.8 %)	0.25
HONO ₂ Dry Deposition / TgN year ⁻¹	21.66 (34.9 %)	21.79 (35.0 %)	0.13
Other Inorganic NO _y Deposition / TgN year ⁻¹	1.21 (2.0 %)	0.96 (1.5 %)	-0.25
PANs / TgN year ⁻¹	2.45 (3.9%)	1.93 (3.1 %)	-0.52
RONO ₂ Deposition / TgN year ⁻¹	1.41 (2.3 %)	2.03 (3.2 %)	0.62
Nitrophenols Deposition / TgN year ⁻¹	0.08 (0.1 %)	0.07 (0.1 %)	-0.01

1410